Theoret. Comput. Fluid Dynamics (1993) 5: 77–106

Theoretical and Computational Fluid Dynamics

On the Numerical Stability of Mixed Finite-Element Methods for Viscoelastic Flows Governed by Differential Constitutive Equations[1]

R.A. Brown, M.J. Szady, P.J. Northey, and R.C. Armstrong

Department of Chemical Engineering, Massachusetts Institute of Technology, Cambridge, MA 02139, U.S.A.

Communicated by D.D. Joseph and M. Renardy

Abstract. Mixed finite-element methods for computation of viscoelastic flows governed by differential constitutive equations vary by the polynomial approximations used for the velocity, pressure, and stress fields, and by the weighted residual methods used to discretize the momentum, continuity, and constitutive equations. This paper focuses on computation of the linear stability of the planar Couette flow as a test of the numerical stability for solution of the upper-convected Maxwell model. Previous theoretical results prove this inertialess flow to be always stable, but that accurate calculation is difficult at high *De* because eigenvalues with fine spatial structure and high temporal frequency approach neutral stability. Computations with the much used biquadratic finite-element approximations for velocity and deviatoric stress and bilinear interpolation for pressure demonstrate numerical instability beyond a critical value of *De* for either the explicitly elliptic momentum equation (EEME) or elastic-viscous split-stress (EVSS) formulations, applying Galerkin's method for solution of the momentum and continuity equations, and using streamline upwind Petrov–Galerkin (SUPG) method for solution of the hyperbolic constitutive equation. The disturbance that causes the instability is concentrated near the stationary streamline of the base flow. The removal of this instability in a slightly modified form of the EEME formulation suggests that the instability results from coupling the approximations to the variables. A new mixed finite-element method, EVSS-G, is presented that includes smooth interpolation of the velocity gradients in the constitutive equation that is compatible with bilinear interpolation of the stress field. This formulation is tested with SUPG, streamline upwinding (SU), and Galerkin least squares (GLS) discretization of the constitutive equation. The EVSS-G/SUPG and EVSS-G/SU do not have the numerical instability described above; linear stability calculations for planar Couette flow are stable to values of *De* in excess of 50 and converge with mesh and time step. Calculations for the steady-state flow and its linear stability for a sphere falling in a tube demonstrate the appearance of linear instability to a time-periodic instability simultaneously with the apparent loss of existence of the steady-state solution. The instability appears as finely structured secondary cells that move from the front to the back of the sphere.

1. Introduction

Numerical simulation of the steady-state and transient flows of viscoelastic polymer melts and solutions has much potential application in the design, optimization, and control of processing

[1] Financial support for this research was given by the National Science Foundation, the Office of Naval Research, and the Defense Research Projects Agency. Computational resources were supplied by a grant from the Pittsburgh National Supercomputer Center and by the MIT Supercomputer Facility.

equipment for a variety of manufacturing and materials processing industries. In the simplest formulations, modeling of these flows requires the solution of the equations of mass and momentum conservation for an incompressible liquid simultaneously with a hyperbolic set of quasilinear differential equations for the extra component of the deviatoric stress tensor due to the viscoelastic behavior of the fluid. Finite-element methods have been developed for the solution of this equation set for all the reasons that make these methods popular for the analysis of Newtonian flows; complex geometries are easily incorporated, nonuniform meshes can be employed to distribute the computational power to regions of the domain where the solution changes rapidly, and the boundary conditions for free-surface flows can be systematically incorporated into the numerical approximation. Even with the large knowledge base built upon Newtonian flow problems, the numerical analysis of viscoelastic flow problems governed by differential constitutive equations have emerged as distinctly difficult problems (Brown *et al.*, 1986). Accordingly, families of new mixed finite-element methods have been developed for calculation of the velocity, pressure, and deviatoric stress fields in viscoelastic flows. Presently, several such methods have been shown to give numerically stable and convergent solutions to steady-state viscoelastic flows, as has been demonstrated for a number of test problems with smooth solutions.

The mixed boundary-value problem governing the two-dimensional transient flow of a viscoelastic liquid described by the prototypical differential constitutive model is written here in terms of the dimensionless velocity ($\mathbf{v}(x)$), pressure ($p(x)$), and deviatoric stress ($\tau(x)$) fields as

$$Re\left(\frac{\partial \mathbf{v}}{\partial t} + \mathbf{v}\cdot\nabla\mathbf{v}\right) = \nabla\cdot\tau + \nabla p + \mathbf{g}(\mathbf{x}), \tag{1}$$

$$\nabla\cdot\mathbf{v} = 0, \tag{2}$$

$$\tau + h(\mathrm{tr}\,\tau; De)\left(\frac{\tau}{f(\mathrm{tr}\,\tau; De)}\right)_{(1)} = -\dot{\gamma} - De\beta\left(\frac{\dot{\gamma}}{f(\mathrm{tr}\,\tau; De)}\right)_{(1)}, \tag{3}$$

where the subscript $\tau_{(1)}$ defines the upper convected derivative of the tensor τ as

$$(\tau)_{(1)} \equiv \frac{D\tau}{Dt} - ((\nabla\mathbf{v})^t\cdot\tau + \tau\cdot(\nabla\mathbf{v})), \tag{4}$$

$\dot{\gamma} \equiv (\nabla\mathbf{v})^t + (\nabla\mathbf{v})$ is the rate-of-strain tensor, and $\mathbf{g}(\mathbf{x})$ is the body force acting on the liquid. The Reynolds number $Re = V^*L^*\rho/\eta_0$ and Deborah number $De = \lambda_0 V^*/L^*$ are defined using the velocity (V^*) and length (L^*) scales used to form the dimensionless variables; stresses and pressure have been made dimensionless using the scale $\eta_0 V^*/L^*$. In these definitions, η_0 is the zero shear-rate viscosity, λ_0 is the zero shear-rate relaxation time, and ρ is the density of the fluid. In the formulation of the constitutive equation, (3), the parameter β is equal to the ratio of the viscosity of a Newtonian solvent (η_s) to the viscosity of the composite solution ($\eta_0 = \eta_s + \eta_p$), where η_p is the viscosity of the polymer; the parameter β plays a pivotal role in the discussion here.

The functions $h(\mathrm{tr}\,\tau; De)$ and $f(\mathrm{tr}\,\tau; De)$ in (3) are specific for different viscoelastic constitutive models. The simplest models are recovered by setting $f = 1$ and $h = De$ to yield the Oldroyd-B model, and, in addition, $\beta = 0$ to give the upper-convected Maxwell (UCM) model. Other models, such as the dumbbell model of Chilcott and Rallison (1988), and the modified UCM model of Apelian *et al.* (1988) are recovered by other suitable choices of the functions $f(\mathrm{tr}\,\tau; De)$ and $h(\mathrm{tr}\,\tau; De)$.

Mixed finite-element methods for the numerical solution of the momentum, continuity, and constitutive equations involve approximations for the velocity, pressure, and deviatoric stress fields and discretization of these equations by appropriate weighted residual methods. Issues in the development of these methods include the relationships between the choice of the weighted residual method for each differential equation and the mathematical type of the equations, as well as the connection between the weighted residual methods and the choice of polynomial spaces for the finite-element approximations.

Guidance in these choices has come from several directions: the theory of the mathematical type of the equation set, (1)–(3) (Rutkevich, 1970, 1972; Joseph *et al.*, 1985), the development of mathematical proofs for the existence of solutions for small De (Renardy, 1985), and the development of rigorous convergence proofs for finite-element approximations in this limit (Baranger and Sandri, 1991a,b) These developments are reviewed in Section 2.

Based on this information and much numerical experimentation, there has been considerable progress in the development of numerically stable and accurate mixed finite elements for viscoelastic flows. Numerically stable and convergent calculations of steady-state, two-dimensional flows have been demonstrated with several formulations using conventional, low-order, finite-element approximations (Marchal and Crochet, 1987; King *et al.*, 1988; Rajagopalan *et al.*, 1990b). Two of these formulations are discussed in detail here: the explicitly elliptic momentum equation (EEME) developed by King *et al.* (1988) for calculations using the UCM model and the elastic-viscous split stress (EVSS) formulation of Rajagopalan *et al.* (1990b) for models with a solvent viscosity, i.e., $\beta \neq 0$. The EVSS formulation also gives convergent solutions for the UCM model, as demonstrated by Rajagopalan *et al.* (1990b) and pursued further here.

Calculations for model flows, such as the flow between eccentric rotating cylinders, the flow through an undulating tube, and the flow around a sphere in a tube have been demonstrated to be convergent with mesh refinement for the simplest viscoelastic constitutive equations, the upper-convected Maxwell and Oldroyd-B equations, and for moderate values of the Deborah number. These solutions have been compared with calculations using spectral finite-element (Beris *et al.*, 1987) and spectral finite-difference methods (Pilitsis and Beris, 1989) to establish the accuracy of the calculations. The accuracy of the calculation of any given flow appears to be limited only by the resolution of thin boundary and internal layers in stress that develop adjacent to solid boundaries and in strong extensional flows. The boundary layers next to solids are particularly important in the discussion here. These thin layers result because of the singular nature of the constitutive equations in the limit where the velocity field vanishes, as at a stationary, no-slip surface. In this limit, which occurs at no-slip surfaces, the constitutive equations reduce from hyperbolic conservation laws to ordinary differential equations in time defined at each point along the boundary. This singularity of the hyperbolic equations is emphasized in the discussion below.

Present finite-element methods still seem far from optimal. Solutions for typical flows show that the stress field requires far more resolution than velocity; however, the present methods appear to have mathematical compatibility constraints that couple the approximations for velocity and stress so as to be inefficient for computing very accurate stress fields. As discussed in Section 2, available theory even suggests that this goal may be unattainable because of the direct coupling between the accuracy of these variables implied by the equation set. Moreover, the temporal accuracy and stability of the discrete equations which result from the spatial discretizations are open issues. Although simulation methods for time-dependent calculations have been developed based on both the EEME (Northey *et al.*, 1990, 1992) and the EVSS formulations (presented here), the utility of these algorithms has been limited by convergence problems for flows with high *De*.

The purpose of this paper is to review the EEME and EVSS finite-element formulations for the solution of steady-state and time-dependent differential viscoelastic models and to demonstrate the numerical instabilities inherent in these methods for computing time-dependent flows. Two test problems are used in the discussion. The numerical stability to two-dimensional disturbances is tested by calculation of the stability of an inertialess, planar Couette flow of a UCM fluid generated by parallel moving and stationary solid surfaces. This problem is particularly well suited as a test problem for transient calculations because the eigenstructure of the linear-stability problem is known in closed form (Gorodstov and Leonov, 1967; Renardy and Renardy, 1986) and because the homogeneous base flow is represented exactly in the finite-element approximations used in the mixed methods described here; hence all difficulties with spatial resolution can be attributed to the approximation of the linearized disturbances. Moreover, in the absence of inertia this flow is stable for any *De*, although the most dangerous disturbance does approach neutral stability with increasing *De*. This feature and the spatial complexity of the eigenfunctions make this linear stability calculation a difficult test for transient simulations.

Recently, Keiller (1992) has used the same linear-stability problem as a test of numerical stability of finite-difference methods for the Oldroyd-B, UCM, and a FENE constitutive equation. He came to the conclusion that the critical value of *De* for the onset of numerical instability for the calculations was a function of the product of the spatial discretization in the streamwise and cross-stream directions. Keiller also implied that the calculations were stabilized by adding either a Newtonian solvent (the Oldroyd-B model) or by adding artificial diffusion to the discretization of the constitutive equation. Our calculations using the streamline upwind (SU) method seem to confirm this latter point.

We see the mesh dependence described by Keiller for the EVSS method; however, it is not present in the EVSS-G formulation described here.

We demonstrate that both the EEME and EVSS methods fail for high values of *De* and predict fictitious numerical instabilities. The eigenfunctions for the most dangerous disturbances are localized near the stationary surface, either a solid surface or at a plane in the flow, depending on the relative motion of the two planes. A modification to the EEME method, EEME-P, is introduced that moves the numerical instability to higher values of *De*. The EEME-P method differs from the EEME formulation only in an *ad hoc* change in the treatment of the pressure field in the momentum equation. The improved temporal stability of this formulation suggests that the numerical instability seen in calculations with the EEME and EVSS methods is a result of incompatibility in the finite-element approximations. We argue that the compatibility of the stress and velocity gradient approximations is an issue, especially near stationary streamlines, such as exist along nonmoving solid boundaries, where the constitutive equation reduces to an algebraic relationship between these two variables.

We describe a new set of mixed finite-element approximations for velocity, velocity gradient, deviatoric stress, and pressure which appear to be compatible in this limit; we call the EVSS formulation that uses these approximations EVSS-G. This mixed set of finite-element approximations is tested with Galerkin's method for the momentum/continuity equation pair and several discretizations for the hyperbolic constitutive equation; these are the SU, SUPG, and the Galerkin least squares (GLS) techniques. The EVSS-G method with the SUPG and SU discretizations is found to be numerically stable for the planar Couette flow up to very high values of *De*. This is a major result of this paper.

The relevance of the numerical instability to the calculation of complex flows is demonstrated by the application of the methods to calculation of the flow of the UCM model for flow around a sphere falling in a tube, a standard test problem for viscoelastic flow simulations. Steady-state calculations with fixed finite-element meshes cease to converge at a maximum value of *De*. We test the numerical stability of these flows by time-integration of the transient equations linearized about the steady-state solution, so that the linear disturbances are represented in the same finite element basis set. Transient analysis for random initial disturbances using the EEME-P formulation predicts that the flow becomes neutrally stable precisely at the point of loss of convergence. The neutrally stable disturbance oscillates in time, suggesting that the discrete evolutionary problem has a time-periodic solution that emanates from this value of *De*. Moreover, the disturbance has fine-scale spatial structure adjacent to the sphere, which is stationary in the calculations. The limited experimental evidence of Bisgaard (1983) suggests an instability in viscoelastic flow around a sphere with fine structure near it, although the loss of existence of the steady-state solution in the calculations makes the conclusions far from definitive.

Several mathematical results for the Oldroyd-B and UCM models relevant to the formulation of numerical methods are summarized in Section 2. A framework for mixed finite-element methods for viscoelastic flows is presented in Section 3 along with the EEME and EVSS mixed methods developed by us and the extension to the EVSS-G mixed methods. Numerical results for the two sample flows are discussed in Sections 4 and 5, respectively.

2. Mathematical Results

The discussion in the remainder of this paper is confined to the special case of inertialess flow, i.e., $Re = 0$, in the equation for conservation of momentum, (1). Note that in this limit, time dependence only enters through the evolutionary term in the constitutive equation. We also confine our calculations to the UCM constitutive equation, although discussion of formulations is presented in more general terms. Rutkevich (1970, 1972) was the first to study the mathematical type of the equation set defining the UCM model. The importance of this analysis and the subsequent study by Joseph *et al.* (1985) lies in the observation that the equation set is of mixed mathematical type. The linearized equation set for steady-state, two-dimensional flow is a set of six first-order partial differential

equations for the canonical variables formed by the two velocity components, the three deviatoric stress components, and the pressure. This equation set has mixed type, i.e., some variables have elliptic character and others are hyperbolic. The character of the velocity field is most clear when the momentum equation is rewritten by substituting the UCM constitutive equation into (1) for $\nabla\cdot\tau$ to yield the *explicitly elliptic momenturn equation* or EEME for inertialess flow ($Re = 0$), as first derived by Renardy (1985):

$$\nabla\cdot(\chi\cdot\nabla\mathbf{v}) + De(\nabla\mathbf{v})\cdot(\nabla\tau) + \nabla q = \mathbf{0}, \tag{5}$$

where χ is the tensor,

$$\chi \equiv De\tau - \delta, \tag{6}$$

and q is the modified pressure field,

$$q \equiv p + De\left(\frac{\partial p}{\partial t} + \mathbf{v}\cdot\nabla p\right). \tag{7}$$

It is straightforward to show that χ is negative definite by using the integral form of the UCM constitutive equation (Dupret *et al.*, 1985). Then, if the EEME/continuity equation pair is viewed as the set for the velocity and pressure fields, (2) and (5) define an elliptic saddle-point problem for the variables q and $\mathbf{v}$. The pressure field p is recovered from this solution by solving (7) as a hyperbolic differential equation. Simultaneously, the UCM constitutive equation can be written as

$$De\left(\frac{\partial\tau}{\partial t} + \mathbf{v}\cdot\nabla\tau\right) + (\tau - De((\nabla\mathbf{v})^t\cdot\tau + \tau\cdot\nabla\mathbf{v})) = -\dot{\gamma}, \tag{8}$$

which describes a set of linear hyperbolic equations for the stress tensor, given the velocity as data. The singularity of the constitutive equation on curves with $\mathbf{v} = \mathbf{0}$ is evident. It is interesting to note that no higher-order derivatives on either τ or p were introduced into the momentum equation through the operation of taking the divergence of the constitutive equation. This results from repeated substitution of the momentum equation to eliminate these terms, which are combined into the definition of q. In fact, this rearrangement removes the higher-order term $\nabla\cdot(\mathbf{v}\nabla p)$ from the momentum equation and a time-derivative of the pressure; we return to this point in Section 3.

The equation set (2) and (5)–(8) represent the EEME formulation first employed by King *et al.*, (1988) in finite-element analysis of viscoelastic flows. Renardy (1985) used this separation into elliptic and hyperbolic parts to bound the differential operators in each part of the problem and to establish a fixed-point iteration to prove the existence of solutions to the UCM model for sufficiently small *De*. His proof relies on smoothness of the velocity field up to the second derivative.

This statement is made more precise by introducing the Sobolev spaces, which are central to the mathematical analysis of finite-element methods for elliptic boundary-value problems (Carey and Oden, 1986). A function $g(\mathbf{x})$ is defined as being square-integrable, or $g(\mathbf{x}) \in L^2(\mathscr{D})$, where $\mathscr{D}$ is the domain, if the norm of $g(\mathbf{x})$ satisfies the condition

$$\|g\| \equiv (g, g)^{1/2} \equiv \int_{\mathscr{D}} g^2\, dA < \infty. \tag{9}$$

The Sobolev spaces $g(\mathbf{x}) \in H^m(\mathscr{D})$ are defined for any integer m as

$$H^m(\mathscr{D}) = \{g(\mathbf{x}) \in L^2(\mathscr{D});\ D^s g \in L^2(\mathscr{D}),\ s = 1, \ldots, m\}, \tag{10}$$

where D^m symbolizes all mth-order partial derivatives of $g(\mathbf{x})$. Equation (10) implies that all mth-order derivatives of $g(\mathbf{x})$ are square integrable and leads naturally to the norm for $H(\mathscr{D})$ defined as

$$\|g\|_1^2 \equiv \int_{\mathscr{D}} [g^2 + |\nabla g|^2]\, dA < \infty \tag{11}$$

with analogous definitions of the norms for higher-order Sobolev spaces. In the context of Sobolev spaces, Renardy's proof of existence requires that $v_i \in H^2(\mathscr{D})$, $q \in H^1(\mathscr{D})$, and $\tau_{ij} \in H^1(\mathscr{D})$. It is interesting that $\tau_{ij} \in H^1(\mathscr{D})$ implies the same smoothness of the stress field in the streamwise and cross-stream directions; this is unnatural for the hyperbolic equations, in which the differential operator only smooths the stress in the streamwise or characteristic direction. These remarks are relevant to the discussion of the continuity of typical finite-element approximations in Section 3.1.

Although the EEME formulation is robust for expressing the ellipticity of the momentum and continuity equations for the UCM constitutive model, it is not appropriate for mathematical analysis or numerical solution with constitutive models that include a solvent viscosity, i.e., $\beta \neq 0$. This point is most clearly seen from the analysis of the mathematical type of the two-dimensional flow for an Oldroyd-B fluid ($h = De$ and $f = 1$ in (1)). Here the added term $\beta\dot{\gamma}_{(1)}$ introduces second-order derivatives in velocity into the constitutive equation and forces the canonical variables to be changed to include velocity gradients instead of velocity. This difference singularly changes the mathematical type of the equation set. The mathematical type is most easily seen by rewriting the equation set in terms of the viscous and elastic or polymer (τ_p) portions of the deviatoric stress tensor defined as

$$\tau \equiv \tau_p - \eta_s\dot{\gamma}. \tag{12}$$

In the variable τ_p, the equation set becomes

$$-\beta\nabla^2\mathbf{v} + \nabla\cdot\tau_p + \nabla p = 0, \tag{13a}$$

$$\nabla\cdot\mathbf{v} = 0, \tag{13b}$$

$$\tau_p + De\tau_{p(1)} + (1-\beta)\dot{\gamma} = \mathbf{0}. \tag{13c}$$

The momentum/continuity pair, (13a) and (13b), form an elliptic saddle-point problem for the velocity and pressure fields, if the elastic stress tensor is viewed as data for the equation set. The ellipticity of (13a) is guaranteed by the appearance of the solvent viscosity multiplying the Laplacian operator; accordingly, we refer to the formulation as the *viscous form* (Rajagopalan *et al.*, 1990). The constitutive equation (13c) is hyperbolic for the components of the elastic stress. Renardy *et al.* (1987) have used this formulation as a basis for constructing a proof of the existence of weak solutions for the Oldroyd-B model for small *De*. Again, a fixed-point iteration was established between the elliptic saddle-point problem and the solution of the constitutive equation. For smooth solutions (the same conditions discussed above apply), bounds on each operator allowed proof of convergence of the fixed-point iteration for sufficiently small *De*. Baranger and Sandri (1991a,b) have used this same approach to prove convergence of finite-element approximations written in the viscous formulation.

Although formally correct for the Oldroyd-B fluid, the elliptic operator in (13a) will become singularly small as the Deborah number is increased and the role of the elastic part of the stress increases. In fact, Rajagopalan *et al.* (1991) have shown that mixed finite-element methods based on the formulation, (13), perform poorly as *De* is increased. This observation motivated these investigators to use a slightly different splitting of the stress tensor which removes β from the momentum equation. This new form is the elastic-viscous split-stress or EVSS and is defined by the elastic stress tensor $\boldsymbol{\Sigma}$ as

$$\boldsymbol{\Sigma} \equiv \tau_p + (1-\beta)\dot{\gamma}, \tag{14}$$

which when introduced into the momentum and constitutive equations yields

$$-\nabla^2\mathbf{v} + \nabla\cdot\boldsymbol{\Sigma} + \nabla p = 0, \tag{15a}$$

$$\nabla\cdot\mathbf{v} = 0, \tag{15b}$$

$$\boldsymbol{\Sigma} + De\boldsymbol{\Sigma}_{(1)} - De(1-\beta)\dot{\gamma}_{(1)} = \mathbf{0}. \tag{15c}$$

Mendelson *et al.* (1982) first used this formulation for finite-element calculations with a second-order fluid, which is an algebraic stress model; Crochet *et al.* (1984) generalized the algorithm to the solution of differential viscoelastic models. Again, the momentum/continuity equation set form an elliptic saddle-point problem for the velocity and pressure and the constitutive equation is hyperbolic in Σ. The dependence on β has been removed from (14a), with the only additional complication being the appearance of the term $\dot{\gamma}_{(1)}$ in the constitutive equation. Because this term involves second-order derivatives of velocity it requires special attention in the numerical formulation. To date, there has been no use of this formulation of the equation set in analysis, although it has the advantage of retaining the elliptic saddle-point problem, (15a) and (15b), for all values of β, including the UCM limit of $\beta = 0$.

Table 1. Summary of three formulations of the viscoelastic flow problem written as (16).

Formulation	Viscous	EEME	EVSS
$\boldsymbol{\sigma}$	$\boldsymbol{\tau}_p$	$\boldsymbol{\tau}$	$\boldsymbol{\Sigma}$
$\mathbf{D}$	$\eta_s\mathbf{I}$	$\boldsymbol{\chi}$	$\mathbf{I}$
$\mathbf{N}(\nabla\mathbf{v}, \boldsymbol{\sigma})$	0	$(\nabla\mathbf{v})\cdot(\nabla\cdot\boldsymbol{\sigma})$	0
q	p	q	p

3. Mixed Finite-Element Methods

We describe mixed finite-element methods in a general context which allows incorporation of the EEME, EVSS, and several new formulations. We consider the general time-dependent statement for two-dimensional, inertialess flow problems posed in the following form:

$$\nabla\cdot(\mathbf{D}\cdot\nabla\mathbf{v}) + De\mathcal{N}(\nabla\mathbf{v}, \boldsymbol{\sigma}) + \nabla q = \mathbf{0}, \tag{16a}$$

$$\nabla\cdot\mathbf{v} = 0, \tag{16b}$$

where $\mathbf{v}$ is the velocity field, q is a generalized pressure, and $\boldsymbol{\sigma}$ is tensorial stress defined by a constitutive equation of the form

$$De\left(\frac{\partial\boldsymbol{\sigma}}{\partial t} + \mathbf{v}\cdot\nabla\boldsymbol{\sigma}\right) + (\boldsymbol{\sigma} - De\mathcal{A}(\nabla\mathbf{v}, \boldsymbol{\sigma})) = -(1-\delta)\dot{\boldsymbol{\gamma}} - (1-\beta)\delta De\dot{\boldsymbol{\gamma}}_{(1)}, \tag{16c}$$

where δ is a constant that is either zero or one and other variables have the definitions given before. The operator $\mathcal{N}(\nabla\mathbf{v}, \boldsymbol{\sigma})$ in (16a) represents the bilinear form that appears in the EEME formulation and the term $\mathcal{A}(\nabla\mathbf{v}, \sigma)$ is the bilinear product of velocity gradients and stress introduced through the upper-convected derivative, as expressed in (4). The tensorial viscosity $\mathbf{D}$ is equal to $\boldsymbol{\chi}$ for the EEME formulation or to the identity tensor otherwise. The viscous, EEME and EVSS forms are recovered from (16) by the substitutions listed in Table 1.

3.1. Finite-Element Approximation Spaces

Mixed finite-element methods are constructed by approximating the variables $(\mathbf{v}, \nabla\mathbf{v}, \boldsymbol{\sigma}, q)$ throughout the computational domain D by expansions of low-order Lagrangian finite-element bases defined on quadrilateral elements denoted as $\{D_i\}$. The finite-element approximations for each variable, expressed as $(\mathbf{v}^h, (\nabla\mathbf{v})^h, \boldsymbol{\sigma}^h, q^h)$ are constructed from the approximation spaces $(\mathbf{V}^h, \mathbf{G}^h, \boldsymbol{\Sigma}^h, Q^h)$, respectively, where each space is defined by the order of the polynomial and the degree of continuity of the approximation between elements. It is important to note that all three formulations collapse in the limit $De = 0$ to the Stokes problem and that the constitutive equation, (16c), decouples from the other equations. For the viscous and EVSS formulations the constitutive equation gives the trivial result for $De = 0$. The well-known compatibility or LBB constraints that must be satisfied by the finite-element approximations for velocity and pressure in the Newtonian limit restrict the choice of approximations for the viscoelastic problem; see Carey and Oden (1986) and Brezzi and Fortin (1991). The work of Baranger and Sandri (1991a,b) suggests that the LBB constraint must be satisfied for the viscous formulation for viscoelastic flows for $De > 0$ as well.

A. Velocity and Pressure. The elliptic saddle-point problem defined by (16) is solved by Galerkin's method using combinations of basis sets for $(\mathbf{v}^h, q^h)$ which are known to be compatible for Stokes flow (Carey and Oden, 1986). The weak solution of such a saddle-point problem gives velocity fields in $H^1(\mathscr{D})$ and pressure fields in $L^2(\mathscr{D})$. In all the calculations described here we use biquadratic Lagrangian polynomials for velocity $(Q_2(\mathscr{D}))$ and continuous bilinear Lagrangian polynomials for pressure $(Q_1(\mathscr{D}))$; discontinuous pressure approximations have also been used by King *et al.* (1988) for the EEME formulation.

B. Deviatoric Stress. The issue of compatibility arises again with the selection of approximating spaces for stress (Σ^h) and velocity gradients (G^h). The coupling of these approximations is most apparent in the Newtonian limit, where the spaces should be equivalent; however, this limit does not directly affect viscoelastic flow simulations with the three formulations presented here because of the decoupling of the constitutive equation from the Stokes problem in the limit $De = 0$. However, a similar situation arises with $De > 0$ on any curve with $\mathbf{v} = \mathbf{0}$, as is seen from the form of the constitutive equation (16c),

$$De\frac{\partial \boldsymbol{\sigma}}{\partial t} + (\boldsymbol{\sigma} - De\mathscr{A}(\nabla\mathbf{v}, \boldsymbol{\sigma})) = -(1-\delta)\dot{\boldsymbol{\gamma}} - (1-\beta)\delta De\dot{\boldsymbol{\gamma}}_{(1)}, \tag{17}$$

in this limit. The smoothing effect of the differential operator $(\mathbf{v}\cdot\nabla\boldsymbol{\sigma})$ has been removed and so the stress tensor is forced to be proportional to $\dot{\boldsymbol{\gamma}}_{(1)}$, which contains second derivatives of the velocity field. In the viscous and EEME formulations, $\delta = 0$, and this proportionality reduces to $\dot{\boldsymbol{\gamma}}$.

For the viscous and EEME formulations, velocity gradients are approximated by formally evaluating the gradients of the finite-element approximations to the velocity field; we label this approximation as $G^h(\mathscr{D}) \equiv DV^h(\mathscr{D})$. Both bilinear and biquadratic Lagrangian approximations to the stress field have been tested, i.e., $\Sigma^h(\mathscr{D}) = Q_1(\mathscr{D})$ and $\Sigma^h(\mathscr{D}) = Q_2(\mathscr{D})$. The viscous formulation with $\Sigma^h(\mathscr{D}) = Q_1(\mathscr{D})$ corresponds to the finite-element method analyzed by Baranger and Sandri (1991b), which has been proved convergent. Interestingly, their analysis gives convergence of the algorithm in a norm containing the errors in the approximations to all the variables $(\mathbf{v}^h, \boldsymbol{\sigma}^h, q^h)$. This estimate would imply that there is no advantage to using higher-order approximations to the stress field. However, this theoretical result is counter to computational experiments for all three formulations, which show that the accuracy of the stress field is much more demanding than the velocity field for even moderate *De*.

The appearance of the second-order velocity derivatives in the EVSS formulation requires approximation of the components of $(\nabla\mathbf{v})^h \equiv \mathbf{G}^h \subset G^h(D)$ to evaluate the term $\dot{\boldsymbol{\gamma}}_{(1)}$; bilinear approximations are used for $\mathbf{G}^h$, i.e., $G^h = Q_1$. We augment the discrete equations described in Section 3.2 with the least-squares approximation

$$(\nabla\mathbf{v}^h - \mathbf{G}^h, \Phi_j^G) = \mathbf{0} \tag{18}$$

which interpolates the discontinuous velocity gradients produced by differentiation of the velocity field onto continuous functions. In the original EVSS method of Rajagopalan *et al.* (1990), these approximations to the velocity gradient were used only in the term $\dot{\boldsymbol{\gamma}}_{(1)}$. We have tested a modified EVSS method in which this continuous approximation is used in the bilinear term $\mathscr{A}(\nabla\mathbf{v}, \boldsymbol{\sigma})$ as well, i.e., $\mathscr{A}(\nabla\mathbf{v}, \boldsymbol{\sigma}) = \mathscr{A}(\mathbf{G}^h, \boldsymbol{\sigma}^h)$. Moreover, the deviatoric stress variable $\boldsymbol{\Sigma}$ is interpolated with continuous bilinear approximations so that interpolation of the stress and velocity gradient are algebraicly equivalent. Accordingly, the finite-element approximations inherent in the constitutive equation are expected to be compatible in the limit $\mathbf{v} = \mathbf{0}$, although no formal proof exists. We refer to this set of finite-element approximations as EVSS-G and discuss predictions of this method in Section 4.

3.2. Weighted Residual Methods

A. Momentum-Continuity Equations. The Galerkin weighted residual equations for the elliptic saddle-point problem, (16a) and (16b), is formed in the usual way to give the equations

$$\int_{\partial\mathscr{D}} \mathbf{n}\cdot(\mathbf{D}\cdot(\nabla\mathbf{v}^h))\cdot\boldsymbol{\delta}_k\, ds - \int_{\mathscr{D}} \nabla\Phi_j^V\cdot(\mathbf{D}\cdot(\nabla\mathbf{v}^h))\cdot\boldsymbol{\delta}_k\, dA$$
$$- \int_{\mathscr{D}} \Phi_j^V\cdot(\mathbf{D}\cdot(\nabla\mathbf{v}^h)^T\colon\nabla\boldsymbol{\delta}_k)\, dA + \int_{\mathscr{D}} \Phi_j^V\cdot(De\mathbf{N}(\nabla\mathbf{v}^h, \boldsymbol{\sigma}^h)\cdot\boldsymbol{\delta}_k)\, dA = \mathbf{0}, \tag{19}$$

$$\int_{\mathscr{D}} \Phi_j^q\cdot(\nabla\cdot\mathbf{v}^h)\, dA = 0, \tag{20}$$

where the finite-element approximations $(\mathbf{v}^h, (\nabla\mathbf{v})^h, \boldsymbol{\sigma}^h, q^h)$ are in the spaces $(V^h, G^h, \Sigma^h, Q^h)$ and the test functions satisfy $(\Phi^v, \Phi^q) \in (V^h, Q^h)$. Equations (19) and (20) are written in general for expressions in

curvilinear coordinates, where δ_k is the unit vector in the kth coordinate direction, which may be a function of position. The line integral in (19) only appears along outflow portions of the domain, and the velocity is assumed to be specified on all solid surfaces and along the inflow boundary.

The EEME-P method was introduced to help alleviate the numerical instability described in Section 4. This formulation differs from the EEME method only in the handling of the modified pressure field, $q(x)$, defined by (7). In the EEME-P formulation the modified pressure is removed, i.e., $q = p$ which reintroduces the terms $\nabla\cdot(\mathbf{v}\nabla p)$ and $\partial p/\partial t$ into the momentum equation. The term $\nabla\cdot(\mathbf{v}\nabla p)$ is integrated-by-parts in the weak form, analogous to (19), and the resulting line integral vanishes on all boundaries with either specified velocity or periodicity. This is the only difference between the EEME and EEME-P formulations.

The viscous formulation is not pursued in the calculations in Sections 4 and 5, because results by Rajagopalan *et al.* (1990) for steady-state flow between eccentric rotating cylinders established that the domain of convergence in *De* was much smaller for the viscous formulation than for the EVSS formulation with reasonable meshes. Mesh-sized wiggles appeared in the results with the viscous formulation for increasing *De* and are an indication that the elliptic stabilization supplied by the operator $\beta\nabla^2\mathbf{v}$ is insufficient at even moderate values of *De* and fixed mesh. This empirical result demonstrates the lack of robustness of the analysis of Baranger and Sandri (1991b), in the sense that their proof is valid in the limits $h \to 0$ and $De \ll 1$ and the numerical calculations evaluate the usefulness of the method outside this limit.

B. Constitutive Equations. Several weighted residual methods are tested for the solution of the quasilinear hyperbolic constitutive equations (16c). These include the Galerkin (GAL), the streamline upwind Petrov Galerkin (SUPG), the streamline upwind (SU), and Galerkin least-squares (GLS) formulations.

Streamline Upwind Petrov Galerkin (SUPG) Method. The SUPG method was originally developed by Brooks and Hughes (1982) and was proved convergent for linear hyperbolic equations by Johnson *et al.* (1984). Here the weighted residual equations are

$$(\psi^\tau, \Sigma + De(\mathbf{v}\cdot\nabla\Sigma + \mathbf{G}^T\cdot\Sigma + \Sigma\cdot\mathbf{G}) - (1-\beta)De(\mathbf{v}\cdot\nabla\mathbf{G} - \mathbf{G}^T\cdot\mathbf{G}^T - 2\mathbf{G}^T\cdot\mathbf{G} - \mathbf{G}\cdot\mathbf{G})) = \mathbf{0}, \quad (21a)$$

where the weighting function Ψ^τ is formed from the finite-element basis for stress components $\Phi^\tau \in \Sigma^h$ as

$$\Psi^\tau \equiv \Phi^\tau + \frac{h\mathbf{v}^h}{\|\mathbf{v}^h\|}\cdot\nabla\Phi^\tau, \quad (21b)$$

where h is a characteristic element size. Normalization of the velocity field is introduced to guarantee that the gradient contribution to the weighting function remains $\mathcal{O}(1)$, regardless of the magnitude of the velocity.

The continuity restrictions necessary for convergence of the SUPG method are not as severe as required by Renardy's existence proof. Johnson *et al.* (1984) showed that SUPG converges for linear first-order hyperbolic equations as long as the dependent variable, $\{\sigma_{ij}\}$, is in the space of functions with square integrable streamwise derivatives, $\sigma_{ij} \in H^1_\psi(\mathscr{D})$, defined analogously to $H^1(\mathscr{D})$, so that $\mathbf{v}\cdot\nabla\sigma_{ij} \in L^2(\mathscr{D})$. There is no guarantee of continuity of the cross-stream derivative of τ_{ij}. It is interesting that the SU method does guarantee smoothness of the derivatives of the stress in all directions, i.e., $\sigma_{ij} \in H^1(\mathscr{D})$, by introducing a second-order operator in the constitutive equation and cross-stream diffusion.

Galerkin (GAL) Method. Galerkin's method applied to the hyperbolic constitutive equation is recovered by setting $h = 0$ in (20). Although Galerkin's method does converge in the L_2-norm to the solution of a linear hyperbolic equation, it gives poor numerical results because no bounds exist on the derivatives of the variable, hence, wiggles in the solution are expected, especially if these are induced by a discontinuity in the data (Johnson *et al.*, 1984). Galerkin's method is applied in Section 4

to the linear stability problem for the plane Couette flow where it performs reasonably well because of the smoothness of the solution. We do not recommend its application in nonlinear flow problems.

Streamline Upwinding (SU) Method. The SU or artificial diffusion method developed by Hughes and Brooks (1982) was used to discretize the constitutive equation using the EVSS-G formulation of the equation set and finite-element approximations. The SU method is expressed in the notation of King *et al.* (1988) by adding the second-order term to the constitutive equation

$$\nabla\cdot(\boldsymbol{\beta}\cdot\nabla\boldsymbol{\tau}_p^h), \tag{22a}$$

where $\boldsymbol{\beta}$ is the artificial diffusivity tensor, which is defined as

$$\boldsymbol{\beta} \equiv \frac{De}{2}\frac{\mathbf{vv}}{|\mathbf{v}\cdot\mathbf{v}|}[(v_x h_x)^2 + (v_y h_y)^2]^{1/2}. \tag{22b}$$

In this expression (v_x, v_y) are the components of the velocity at the center of a quadrilateral element and (h_x, h_y) are the sizes of the element in the x- and y-directions. Because this method gives only $O(h)$ accuracy in the L_2-norm, the use of higher-order polynomials for approximating stress is not justified; hence, we use bilinear approximations for stress and the velocity gradient in the EVSS-G formulation. Marchal and Crochet (1987) used the SU method in their successful mixed formulation for viscoelastic flows.

Galerkin Least-Squares (GLS) Method. Recently, GLS methods have received attention for solving convection-dominated transport problems (Hughes *et al.*, 1989; Franca *et al.*, 1992) and for calculation of viscoelastic flows (Baaijens, 1992; Leborgne, 1992). This method has been proved convergent for linear hyperbolic equations (Leborgne, 1992). In these weighted residual methods, the weak form generated by Galerkin's method is augmented by the term generated by a least-squares approximation, weighted by a factor that depends on the mesh. The purpose of the added component of the residual equation is to give numerical stability to the otherwise unstable Galerkin formulation, while not destroying the consistency of the discretization. We apply the GLS formulation developed by Leborgne (1992) for linear hyperbolic equations to the solution of the constitutive equations. A steady-state hyperbolic operator acting on the stress tensor σ can be defined from (16c) as

$$\mathscr{L}(\boldsymbol{\sigma}) \equiv \boldsymbol{\sigma} + De(\mathbf{v}\cdot\nabla\boldsymbol{\sigma} - \mathbf{A}(\nabla\mathbf{v}^h, \boldsymbol{\sigma})). \tag{23}$$

The weighting function Ψ^τ is formed by adding the basis function to the least-squares residual for the operator in (23) as

$$\Psi^\tau \equiv \Phi^\tau + \delta(\Phi^\tau + De(\mathbf{v}\cdot\nabla\Phi^\tau - A(\nabla\mathbf{v}^h, \Phi^\tau))), \tag{24a}$$

where the scalar δ is defined as

$$\delta \equiv \frac{[(v_x h_x)^2 + (v_y h_y)^2]^{1/2}}{2\|\mathbf{v}\|} \tag{24b}$$

and the components of the velocity and the element size are defined as in (22b). The GLS method has been implemented with the restriction that $\delta \leq 1/24$, as argued by Franca *et al.* (1992).

3.3. Solution of Steady-State and Time-Dependent Problems

Discretization of steady-state problems leads to large sets of nonlinear algebraic equations for the coefficients in the finite-element approximations $(\mathbf{v}^h, (\nabla\mathbf{v})^h, \boldsymbol{\sigma}^h, q^h)$. For each formulation, this set is solved by Newton's method in which the elements of the Jacobian matrix are computed by one-sided finite-difference approximations, and a frontal implementation of asymmetric **LU** decomposition is used to solve the large set of linear equations that result at each Newton iteration (Burdette *et al.*, 1989).

The discretized equations formed by (19), (20), and the constitutive equation constitute a set of differential-algebraic equations for the unknown, time-dependent coefficients in the finite-element approximations $(\mathbf{v}^h, (\nabla\mathbf{v})^h, \boldsymbol{\sigma}^h, q^h)$. We solve this set by fully implicit time integration, as first introduced by Northey *et al.* (1990). We use a first-order accurate Adams–Moulton method.

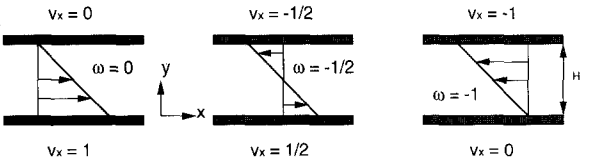

Figure 1. Schematic of planar Couette flow geometry showing the parameter ω for varying the motions of the surfaces.

4. Stability of the Planar Couette Flow

The numerical stability characteristics of the finite-element methods described above were tested by calculation of the linear stability of the planar Couette flow, as shown in Figure 1. Here the steady-state flow is rectilinear with a constant velocity gradient and constant stresses. Using the velocity of the solid surface V as the velocity scale and the gap between the planes H as the length scale gives the viscometric flow for the UCM model as

$$(v_x, v_y) = (1 - y + \omega, 0), \qquad (\tau_{xy}, \tau_{xx}, \tau_{yy}, p) = (1, -2De, 0, 0), \tag{25}$$

where ω is a parameter that fixes the velocities of the two solid surfaces; see Figure 1. For $\omega = 0$, the lower plate is in motion at unit speed and the upper plate is stationary; Keiller's calculations (1992) used $\omega = -1/2$.

Linear stability analysis of the inertialess flow was presented by Gorodstov and Leonov (1967), who showed the presence of both discrete and continuous contributions to the eigenspectrum. For linear disturbances with spatial structure $g(y)e^{(ikx+\sigma t)}$, they showed that the continuous spectrum is composed of eigenvalues (σ_{cont})

$$Re(\sigma_{\text{cont}}) = -\frac{1}{De} \quad \text{and} \quad |\text{Im}(\sigma_{\text{cont}})| \leq k, \tag{26}$$

where k is the spatial wave number in the flow direction. In addition, the discrete spectrum has eigenvalues that occur in pairs for each wave number k; see Gorodstov and Leonov (1967) for the formulas. Most importantly, for $De \gg 1$, the real parts of these eigenvalues (σ_{disc}) approach $-1/2De$ and the imaginary parts approach 0 and k. Thus, as De is increased, members of both the discrete and continuous spectrum move closer to neutral stability, i.e., $Re(\sigma)$ approaches zero; hence, calculations with high De are expected to be more susceptible to numerical instability if the spatial structure of the associated eigenfunctions is not adequately resolved. This difficulty with numerical approximation has plagued attempts at a numerical solution to the eigenvalue problem with inertia (Lee and Finlayson, 1986; Renardy and Renardy, 1986).

The eigenfunctions corresponding to the discrete spectrum are most dangerous because $Re(\sigma_{\text{disc}}) > Re(\sigma_{\text{cont}})$. The difficulty with adequate spatial resolution of these functions is most clear from the form of the cross-stream component of the velocity (v_y) associated with each member of the discrete spectrum (Gorodstov and Leonov, 1967):

$$v_y(x, y, t) = V_k(y)\sigma^{ikx-\sigma t}, \tag{27a}$$

where

$$V_k(y) = \mathbf{c}_{1k}(y - \sigma)e^{ky} + c_{2k}(y - \sigma)e^{-ky} + c_{3k}e^{-kDey(i-c_0)} + c_{4k}e^{-kDey(c_0+i)} \tag{27b}$$

for $\omega = 0$, and $\{c_0, c_{ik}\}$, $i = 1, \ldots, 4$, are constants computed from the boundary conditions and $c_0 \equiv \sqrt{1 + De^{-2}}$. For $k \gg 1$ or $De \gg 1$, the disturbance contains roll cells both in the cross-stream and the flow directions. Fine scale structure is expected in the velocity field across the gap because of the terms proportional to e^{-ikDey} for $k \gg 1$. Moreover, the terms proportional to e^{-ky} and e^{ky} result in boundary layers near both the moving ($y = 0$) and the stationary ($y = 1$) boundaries for $k \gg 1$. The structure of $V_4(y)$ is shown as a three-dimensional surface in Figure 2 for $De = 1$ and $t = 0.1$. The disturbance is concentrated near the stationary boundary and the cellular structure along this boundary is obvious. It is interesting that this eigenfunction is trivial to compute only for low values of De, because round-off error becomes a factor for increasing values of De and k.

The form of (27) and the asymptotic behavior of the eigenvalue suggests that numerical approximation of the linear dynamics for the UCM flow will be extremely difficult for high De and k. The value

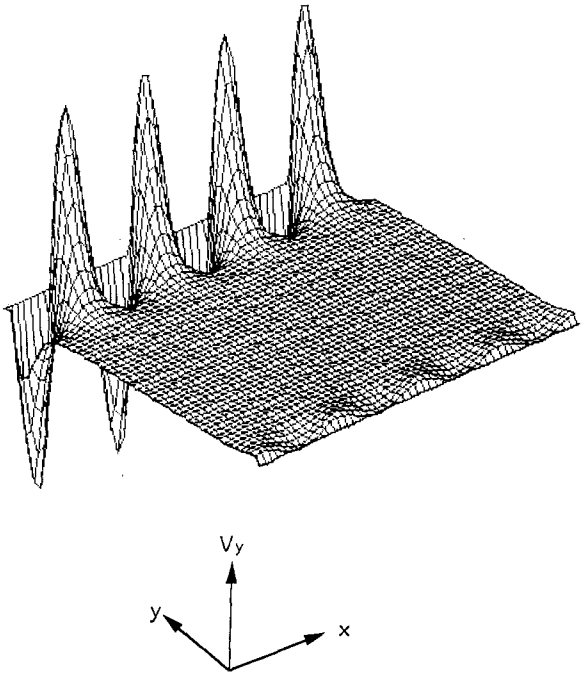

Figure 2. Contour plot of the eigenfunction, (27), for $k = 4$ and $t = 0.1$ from the result of Gorodstov and Leonov (1967).

of the wave number inherent to the finite-element analysis of the calculations is set by the number of elements used in the streamwise direction; the larger the number of elements in this direction, the better the resolution of the spatial structure of the eigenfunction and the more complex the spatial structure of the eigenfunction that can be resolved. Moreover, the temporal response also becomes more complex, because the frequency of the slowly decaying oscillation approaches k.

Computations of the linear stability of the planar Couette flow are carried out by solving the finite-element equations numerically linearized about the base flow, (25). The disturbances are assumed to vanish on the solid surfaces and to be periodic in the streamwise or x-direction; the dimensionless streamwise dimension of the computational domain is set to 1, i.e., the same as the gap width, so that the smallest value k that appears in the domain is $\pi/2$. Results are shown both as contours of the solution components as a function of time and as the evolution of the magnitude of the solution $\mathbf{b}(t)$ of the linearized equations, defined as

$$L_2(\mathbf{b}(t)) \equiv \sqrt{\sum_{i=1}^{N} [b_i(t)]^2}, \tag{28}$$

where $\{b_i(t)\}$ are the components of the solution vector. Transient simulations are started from random initial conditions for the stress and zero initial values for velocity and pressure. The most dangerous eigenfunction, i.e., the one with eigenvalue with the largest real part, will dominate the numerical solution as the solution evolves in time. The real and imaginary parts of the corresponding eigenvalue are estimated from the long time behavior of $L_2(\mathbf{b}(t))$; this procedure was used by Northey *et al.* (1991) to compute the onset of oscillatory instability in the Taylor–Couette flow of a UCM fluid.

Calculations are presented in Sections 4.1–4.7 for each of the finite-element mixed methods described in Section 3. All of these results were carried out using the fixed time step of $\Delta t = 0.1$ in the numerical integration. The numerical stability characteristics of the methods with changing Δt are discussed in Section 4.4.

4.1. EEME/SUPG and EEME/GAL Methods

Calculations for the UCM model were carried out using the EEME/SUPG method, as described in Section 3 with different finite-element meshes and values of *De*. Unless stated otherwise, the meshes

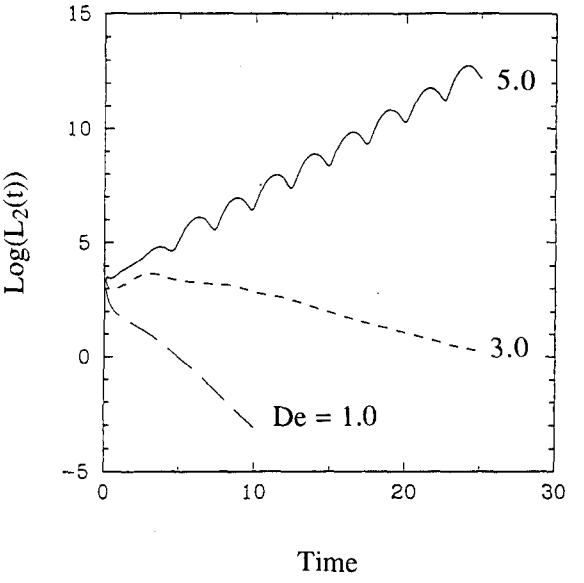

Figure 3. Transient response computed with the EEME/FEM of the amplitude $L_2(t)$ defined by (28) as a function of De for the mesh $N_{el} = 14$ and $\Delta t = 0.1$. Calculations are for the UCM model.

were all square with $N_{el} \times N_{el}$ elements in each direction. The evolution of the amplitude of the disturbance is shown in Figure 3 as a function of the Deborah number for $1 \leq De \leq 5$, $N_{el} = 14$, $\omega = 0$, and $\Delta t = 0.1$. The results for $De = 1$ and $De = 3$ show the exponential decay expected for the linear stable flow; moreover, the slopes of the curves agree approximately with the result of Gorodstov and Leonov (1967) for the real part of the slowest decaying eigenvalue, $-1/2De$. The contours of components of the eigenfunction for v_y and τ_{yy}, corresponding to this mode are shown in Figure 4. The "energy" in the disturbance, defined by the L_2-norm, (28), is concentrated near the stationary boundary and appears to have the longitudinal wave number $k = 28\pi$, which is the maximum value that can be resolved by the mesh with $N_{el} = 14$, assuming that two finite elements are requiled to approximate one flow cell in the disturbance. Thus, as expected from the analysis of Gorodstov and Leonov (1967), the most dangerous disturbance corresponds to the highest wave number k.

At $De = 5$, the behavior of the linear-stability problem is qualitatively different; a discrete eigenmode becomes temporally unstable, as seen by the exponential growth shown in Figure 3. This mode

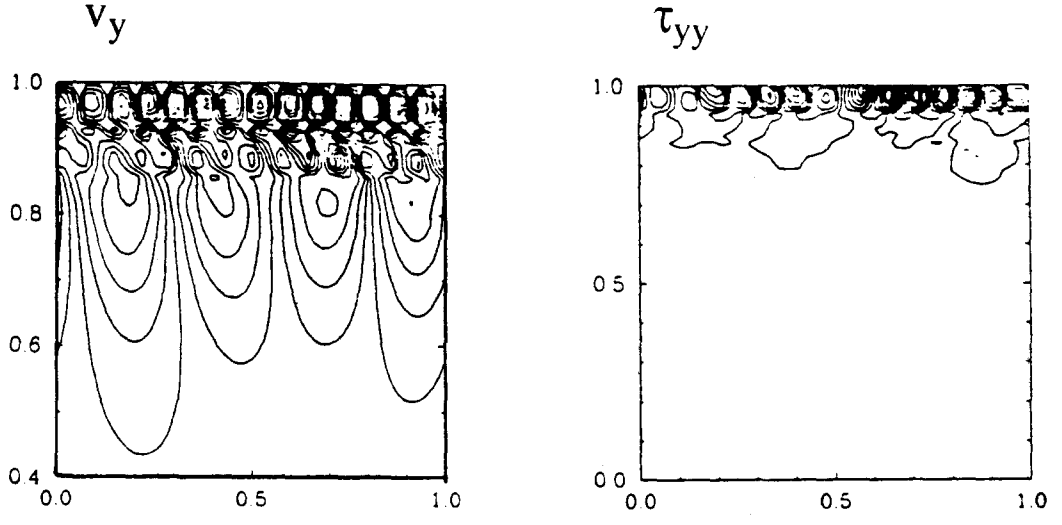

Figure 4. Contours of v_y and τ_{yy} at $t = 10.0$ for $De = 1$ computed with the EEME/SUPG with $N_{el} = 14$ and $\Delta t = 0.1$. This eigenfunction is stable in time, as indicated in Figure 3.

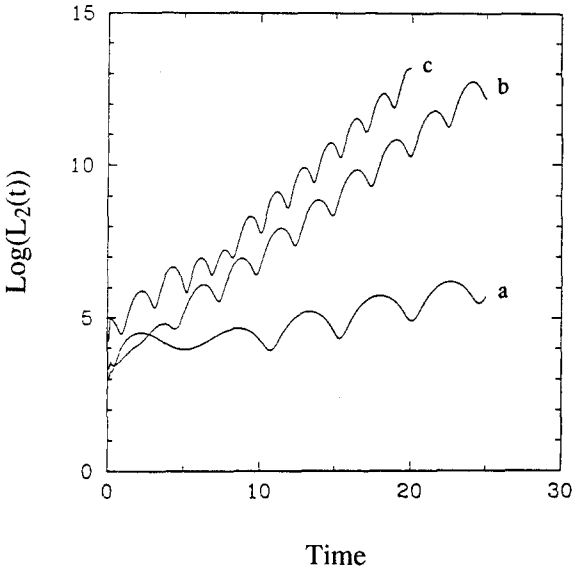

Figure 5. Transient response computed with the EEME/SUPG of the amplitude $L_2(t)$ defined by (28) as a mesh size for $De = 5.0$ and $\Delta t = 0.1$. Calculations are for the meshes with N_{el} equal to (a) 10, (b) 14, and (c) 28.

is fictitious, because the continuous problem admits no instability. Increasing the spatial discretization did not improve the numerical stability of the linear-stability problem. Indeed, using finer meshes produce spurious eigenmodes that grew faster than those for a coarser mesh, as indicated in Figure 5 by the history of the L_2-norm as a function of time for three meshes, $\Delta t = 0.1$ and $De = 5$. The components of the most unstable eigenfunction, as determined for the mesh with $N_{el} = 28$, are shown in Figure 6; again the disturbance has the form of the highest wave number (56π) that is resolvable by the mesh and has energy concentrated near the stationary surface. Also, the frequency of the oscillations in the disturbance, as shown in Figure 5, increases with the mesh refinement; however, the frequency is well below the value $\mathrm{Im}(\sigma_{disc}) = 56\pi$ expected for the most dangerous eigenfunction on this mesh. This is not unexpected, because the time step $\Delta t = 0.1$ does not allow resolution of this frequency.

The numerical instability displayed in Figures 3–6 results from the coupling between the constitutive equation and the elliptic saddle-point problem. This is demonstrated by integrating the linear

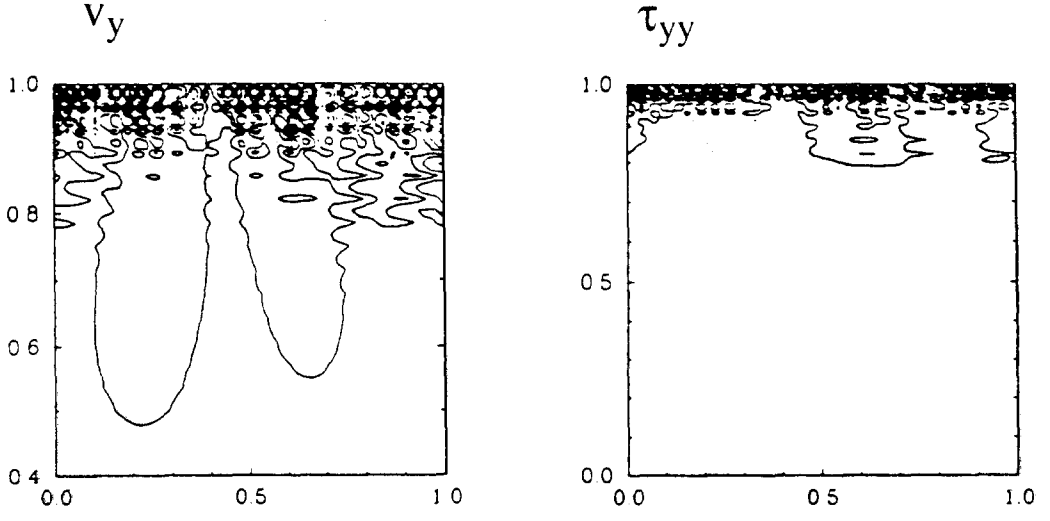

Figure 6. Components of v_y and τ_{yy} at $t = 20.0$ for $De = 5$ computed with the EEME/SUPG with $N_{el} = 28$ and $\Delta t = 0.1$. This eigenfunction is unstable in time, as indicated in Figure 5.

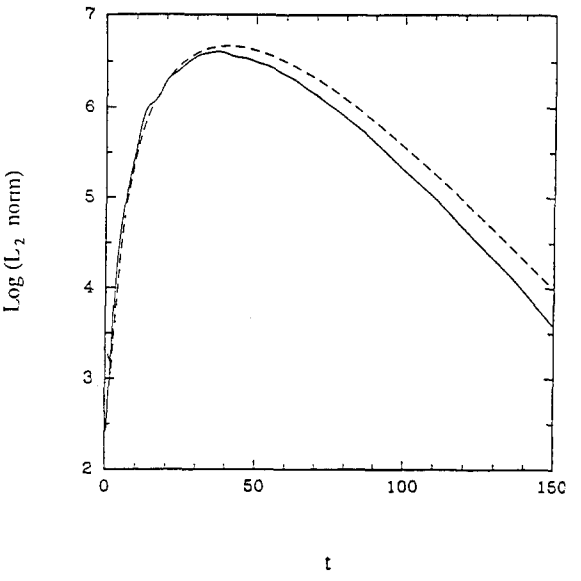

Figure 7. Transient response computed with the EEME/SUPG (---) and EEME/GAL (——) methods of the amplitude $L_2(t)$ defined by (28) for $De = 20.0$ and $\Delta t = 0.1$. Calculations are for the UCM model with the kinematics held fixed so that only components of the stress tensor evolve in time; $N_{el} = 10$.

UCM constitutive equation for the planar Couette flow with the kinematics fixed as the rectilinear base flow. The results for $L_2(t)$ are shown in Figure 7 for $De = 20$ computed by integration using both the SUPG and Galerkin methods with the mesh $N_{el} = 10$ and $\Delta t = 0.1$. As expected from the form of the constitutive equations, the response is a decaying exponential with slope of approximately $-1/De$. Although both methods give very similar values of $Re(\sigma)$, the eigenfunctions are distinctly different and are an excellent demonstration of the qualitative differences in the solution of hyperbolic equations by the SUPG and Galerkin methods. The component of τ_{xx} computed by the two techniques at $t = 150$ is shown in Figure 8. The SUPG method produces a solution that is streamwise (x-direction) smooth everywhere except near the stationary boundary, where the velocity vanishes; here small oscillations appear along the boundary. The solution computed by Galerkin's method (Figure 8(b)) has undulations throughout the solution, a clear indication of the spatial instability that is inherent to this method; see Johnson *et al.* (1984).

The concentration of the energy of the most dangerous disturbance near the zero streamline in the

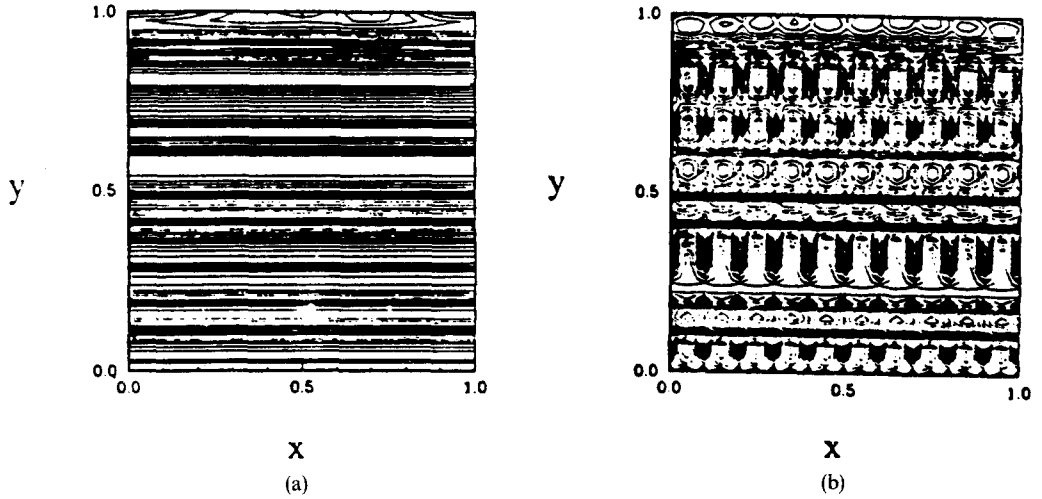

Figure 8. Components of τ_{xx} at $t = 150.0$ for $De = 20$ corresponding to the solutions for the calculations with the fixed kinematics shown in Figure 6; calculations with the (a) SUPG and (b) Galerkin methods are shown. Note that the SUPG method gives results that are streamwise smooth, whereas the Galerkin method does not.

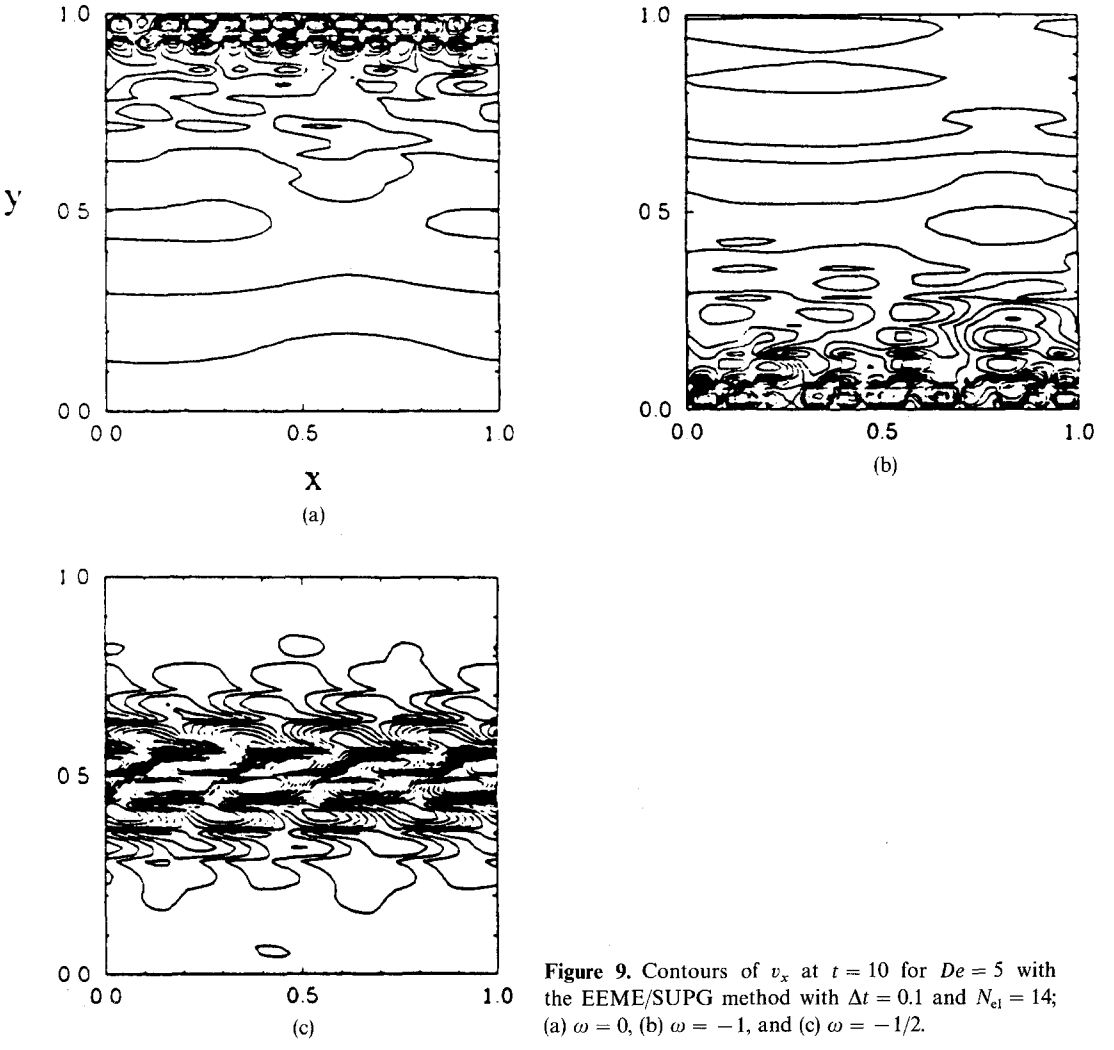

Figure 9. Contours of v_x at $t = 10$ for $De = 5$ with the EEME/SUPG method with $\Delta t = 0.1$ and $N_{el} = 14$; (a) $\omega = 0$, (b) $\omega = -1$, and (c) $\omega = -1/2$.

base flow was emphasized by linear stability calculations with the EEME/SUPG method in which the stationary surface was varied by changing the parameter ω to vary the line of vanishing base velocity from the top boundary ($\omega = 0$; $y = 1$) to the bottom boundary ($\omega = -1$; $y = 0$) and to the midplane ($\omega = -1/2$; $y = 1/2$). For $De = 5$ and $N_{el} = 14$, the response of $L_2(t)$ was identical for all three calculations; however, the concentration of the energy in the eigenfunction was different. As shown by the plots of the contours of v_x in Figure 9, the energy was concentrated near the stationary streamline in the base flow, whether it corresponded to a solid boundary or to the midplane of the flow.

Finally, the boundary conditions on the base flow were changed to be

$$v_x(x, 0) = 2 \quad \text{and} \quad v_x(x, 1) = 1 \tag{29}$$

to study the linear stability of a flow without a stationary streamline. The response of $L_2(t)$ is shown in Figure 10 for $De = 5$, $N_{el} = 14$, and $\Delta t = 0.1$. Components of the eigenfunction are shown in Figure 11 for discretization of the constitutive equation using both the EEME/GAL and EEME/SUPG methods. Both techniques give the correct decaying exponential; however, the most dangerous eigenfunction for the EEME/SUPG method is not concentrated near any boundary and has no streamwise structure at all and thus is not characteristic of any of the eigenfunctions described by Gorodstov and Leonov (1967). The form of the most dangerous eigenfunction has been changed by making a change in the frame of reference of the numerical method.

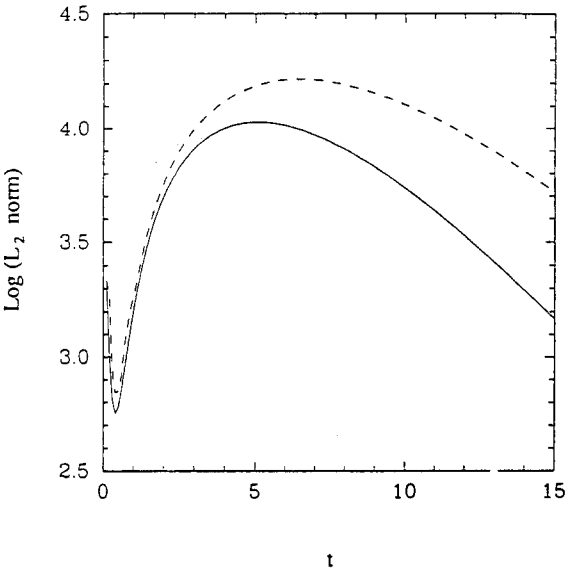

Figure 10. Transient response of the amplitude $L_2(t)$ defined by (28) as computed with the EEME/SUPG (– – –) and the EEME/GAL (——) methods with the boundary condition (29); $N_{el} = 14$, $De = 5.0$, and $\Delta t = 0.1$.

4.2. EVSS/SUPG Method

The numerical stability of the EVSS/SUPG method was tested using the planar Couette flow of a UCM fluid in a manner similar to the calculations described above for the EEME/FEM method. The response of $L_2(t)$ for $De = 3$ and $De = 5$ is shown in Figure 12 for $\omega = 0$, $N_{el} = 14$, and $\Delta t = 0.1$. Just as for the EEME/FEM, the method is numerically stable for $De = 3$ and unstable for $De = 5$. The frequency of oscillation and the critical value of De for the instability are approximately the same as those predicted by the EEME/SUPG method; moreover, the energy of the eigenfunction also is concentrated near the stationary boundary ($y = 1$), as shown in Figure 13.

4.3. EEME-P/SUPG and EEME-P/GAL Methods

The EEME-P/SUPG and EEME-P/GAL methods were tested for computation of the stability of the planar Couette flow for the UCM model in an identical way to that described above for the

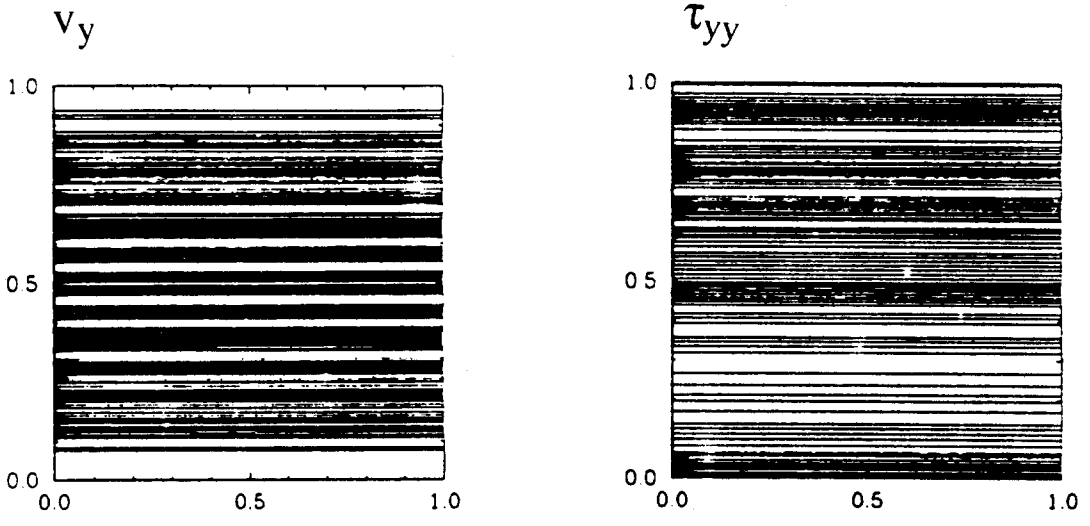

Figure 11. Components of v_y and τ_{yy} at $t = 20.0$ for $De = 5$ computed with the EEME/SUPG method and the boundary condition (29); $N_{el} = 28$ and $\Delta t = 0.1$. This eigenfunction is stable in time, as indicated in Figure 10.

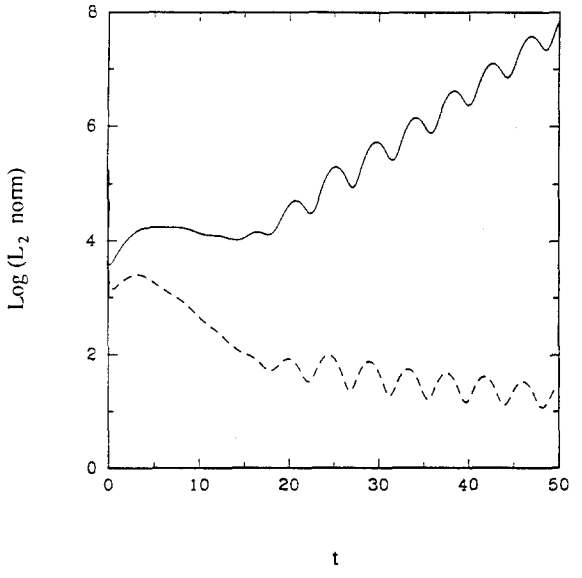

Figure 12. Transient response, computed with the EVSS/SUPG method, of the amplitude $L_2(t)$ defined by (28) as a mesh size for $De = 3.0$ (---) and $De = 5.0$ (——) with $\Delta t = 0.1$. Calculations are for meshes with N_{el} equal to 14.

EEME/SUPG formulation. The plot of $L_2(t)$ for $De = 5$, $\omega = 0$, and $\Delta t = 0.1$ is shown in Figure 14 for meshes with both N_{el} values of 14 and 28. The numerical instability seen in the EEME methods has been removed and all the calculations appear to decay with a rate very similar to $-1/2De$. Components of the eigenfunction for the calculation with $N_{el} = 28$ and the EEME-P/SUPG method are shown in Figure 15 for $t = 50$. Again the energy in the disturbance is concentrated near the stationary boundary ($y = 1$), although a large-scale structure in the velocity field is discernible. Linear stability calculations were stable with the EEME-P method up to $De = 10$ with the time evolution of $L_2(t)$ and the eigenfunction behaving similarly to the forms depicted in Figures 14 and 15.

4.4. EVSS-G/SUPG Method

The EVSS-G/SUPG method uses bilinear Lagrangian interpolation for the velocity gradient field in all terms in the constitutive equation and bilinear interpolation for the components of the elastic stress tensor Σ. The temporal stability of this method was tested by calculation of the linear stability

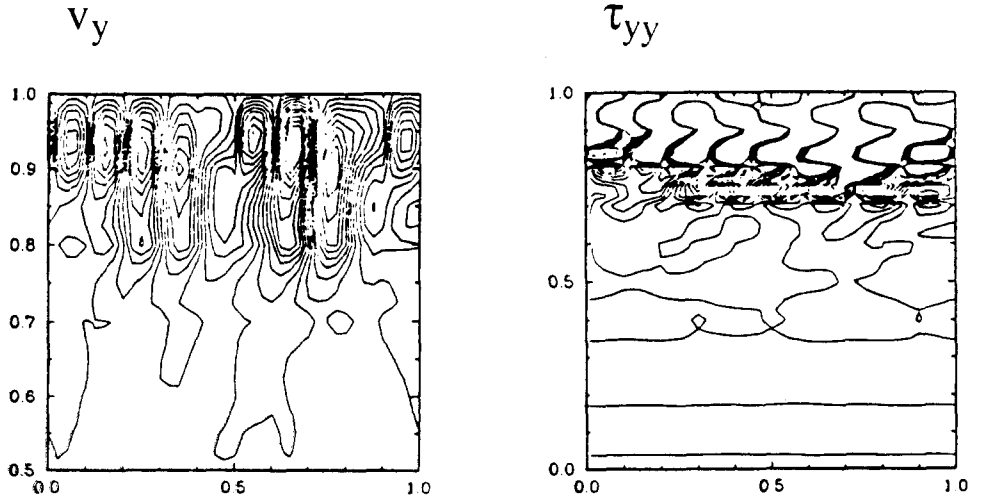

Figure 13. Components of v_y and τ_{yy} at $t = 15.0$ for $De = 5$ computed with the EVSS/SUPG method with $N_{el} = 28$ and $\Delta t = 0.1$. This eigenfunction is unstable in time, as indicated in Figure 12.

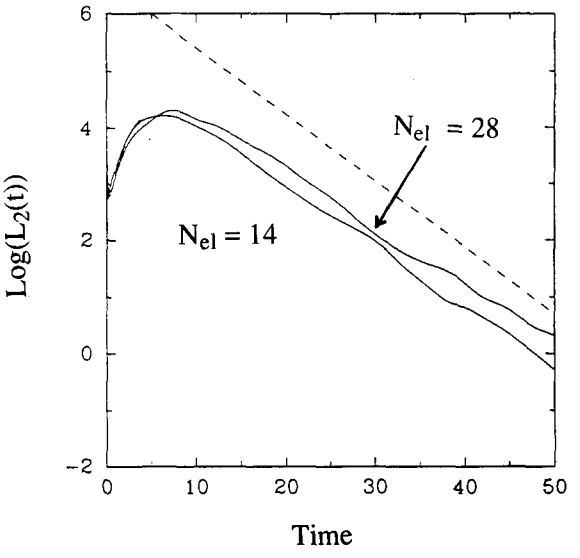

Figure 14. Transient response, computed with the EEME-P/SUPG method, of the amplitude $L_2(t)$ defined by (28) as a function of De for meshes with $N_{el} = 14$ and $N_{el} = 28$; $\Delta t = 0.1$.

of the planar Couette flow, exactly as described above. The most significant result is that the EVSS-G/SUPG method appears to be numerically stable to very high values of De for fixed finite-element discretization. The response of the energy of the disturbance, $L_2(t)$, with time is shown in Figure 16 for calculations with $\omega = 0$ and $\Delta t = 0.1$; calculations are shown for (a) $De = 10$ and (b) $De = 50$ for both a mesh with 4 elements in the streamwise and 10 elements in the cross-stream directions and for a mesh with $N_{el} = 10$ elements in both directions. The calculations with both meshes are numerically stable; however, results with the finer mesh give a better approximation to the correct decay rate of $-1/2De$.

The evolution of the energy of the disturbance for a sequence of calculations with $5 \leq De \leq 50$ is shown in Figure 17 for the 4×10 mesh with $\Delta t = 0.1$. The behavior reproduces the analytical eigenvalue for long time. Although the calculations were stable and accurate for $De = 50$, they were not continued to higher values of De because of the long simulation times associated with the slow decay rate for the disturbances. The contours of the eigenfunction for $V_y(x, y, t)$ at $t = 50$ are shown in

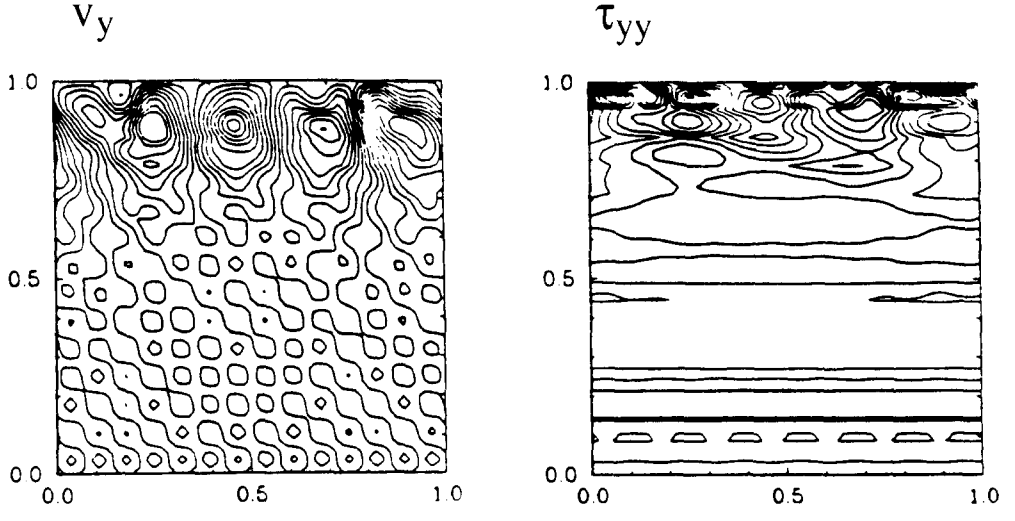

Figure 15. Components of the disturbance to the velocity and stress field at $t = 50.0$ for $De = 5$ computed with the EEME-P/SUPG method with $N_{el} = 14$ and $\Delta t = 0.1$. This eigenfunction is stable in time, as indicated by Figure 14.

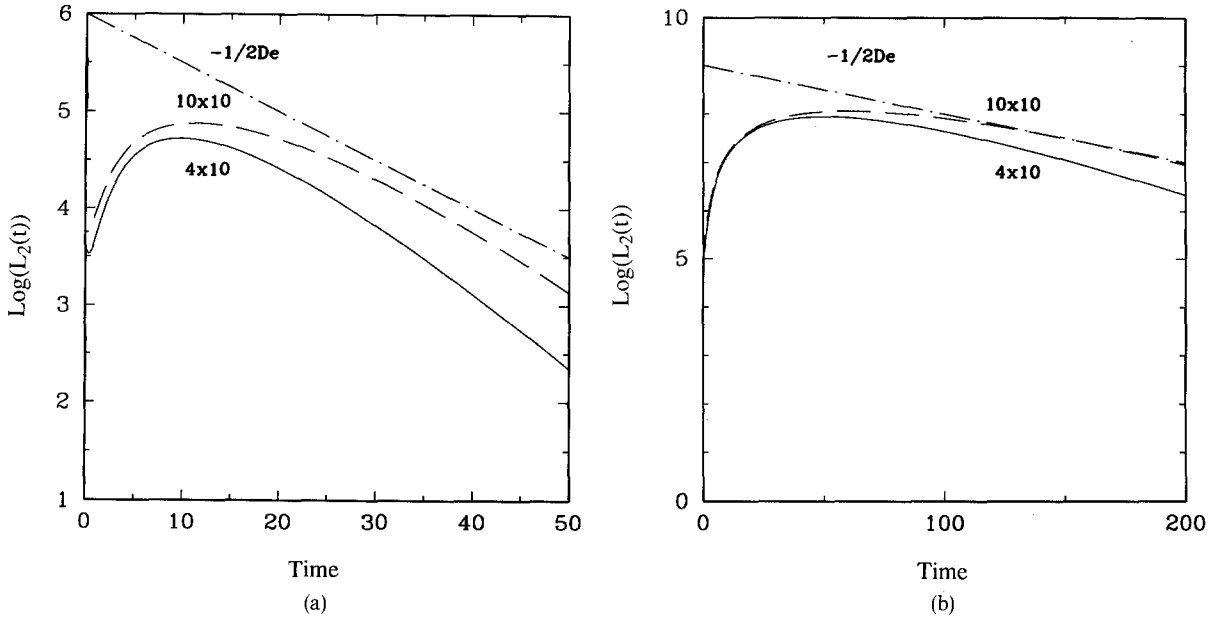

Figure 16. Effect of varying resolution of mesh in the x- and y-directions on temporal stability as computed with the EVSS-G/SUPG method. Results are shown for $(N_x, N_y) = (4, 10)$ and $(10, 10)$ with $\Delta t = 0.1$; (a) $De = 10$ and (b) $De = 50$.

Figure 18, as computed with $N_{el} = 10$ and $De = 10$. The structure of the eigenfunction matches what is expected from the theory.

The behavior of the energy of the disturbance with decreasing time steps is shown in Figure 19 and clearly demonstrates the temporal stability of the EVSS-G/SUPG method; decreasing Δt by a factor of 200 leads to simulations with almost the identical decay rate for the disturbance. However, the oscillation frequency of the disturbance does depend on Δt. This is not unexpected because this temporal frequency approaches k, the streamwise wave number, for large De; k is approximately 8π for the 4×10 mesh. The finest two time steps $\Delta t = 0.05$ and $\Delta t = 0.005$ resolve this frequency, but the largest time step ($\Delta t = 0.1$) does not. The results for the finest two time steps are very similar.

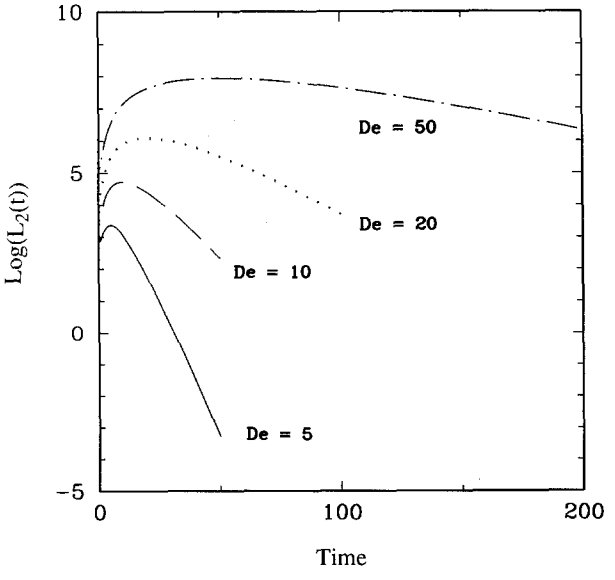

Figure 17. Transient responses, computed with the EVSS-G/SUPG method, of the amplitude $L_2(t)$ defined by (28) are shown for $(N_x, N_y) = (4, 10)$ and $5 \leq De \leq 50$, as computed with $\Delta t = 0.1$.

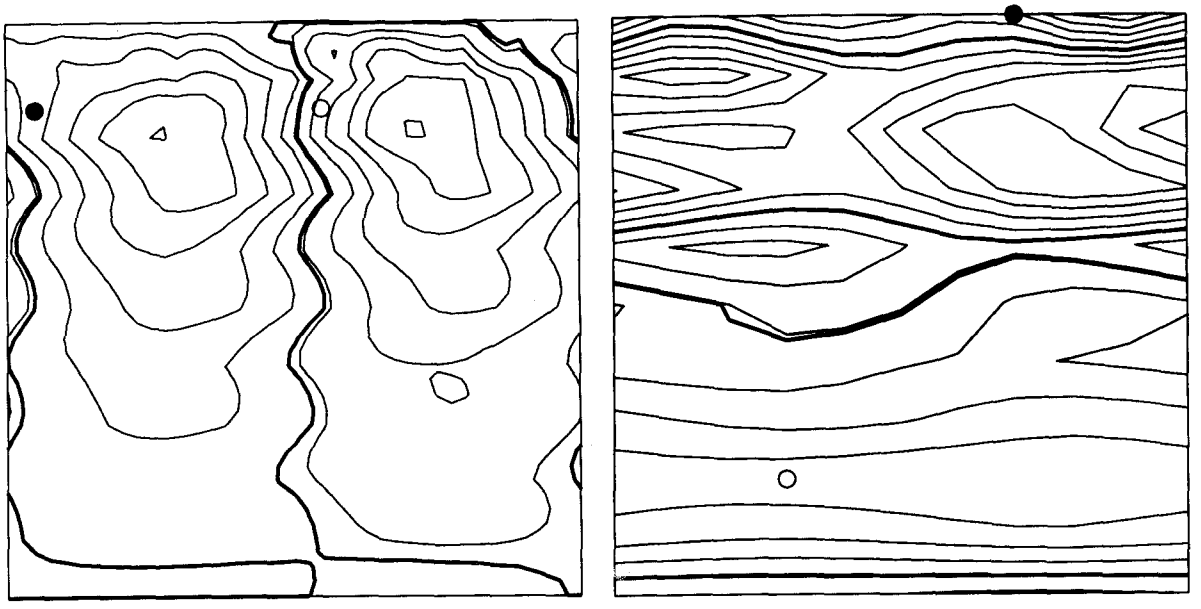

Figure 18. Components of the disturbance to the velocity (v_y) and stress (Σ_{yy}) field at $t = 25.0$ for $De = 10$ computed with the EVSS-G/SUPG method with $N_{el} = 10$ and $\Delta t = 0.1$; this calculation is temporally stable. Maximum and minimum values of the functions are shown.

4.5. EVSS-G/SU Method

Calculations with the EVSS-G/SUPG method clearly demonstrate the improved stability of this formulation over the equivalent method, but without the approximation for the velocity gradient. We demonstrate that this stability is a characteristic of the finite-element approximations to the variables and can be reproduced using any of the methods described in Section 3 for solving the hyperbolic constitutive equation. The SU method was used to discretize the constitutive equation with the EVSS-G formulation of the equation set. The resulting method, referred to as the EVSS-G/SU

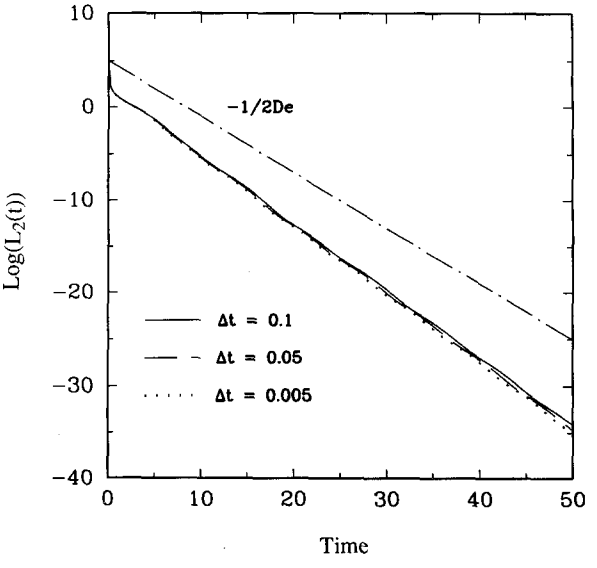

Figure 19. Effect of time step on the evolution of the energy of the disturbance $L_2(t)$ for the EVSS-G/SUPG method with $(N_x, N_y) = (4, 10)$ and $De = 1$. Results are shown for $0.005 \leq \Delta t \leq 0.1$.

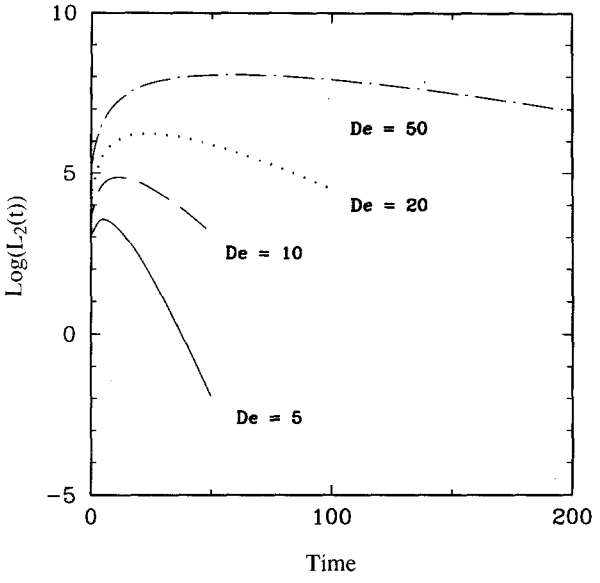

Figure 20. Transient response, computed with the EVSS-G/SU method, of the amplitude $L_2(t)$ defined by (28) as a function of De for the mesh $N_{el} = 10$ and $\Delta t = 0.1$.

technique, had enhanced linear stability for the planar Couette flow, as demonstrated by the evolution of $L_2(t)$ in Figure 20 for $\omega = 0$, $N_{el} = 10$, and $\Delta t = 0.1$. The EVSS-G/SU method has similar numerical stability characteristics to the EVSS-G/SUPG method; the time-dependent calculations for the linear-stability problem reproduce the response expected from the analytical solution up to high values of De. The most dangerous disturbance computed for $De = 50$ and $t = 200$ is shown in Figure 21. The concentration of the energy toward the stationary boundary is still apparent; however, the energy seems to be spread more uniformly in the cross-stream direction, possibly because of the effect of the cross-stream diffusivity in the method.

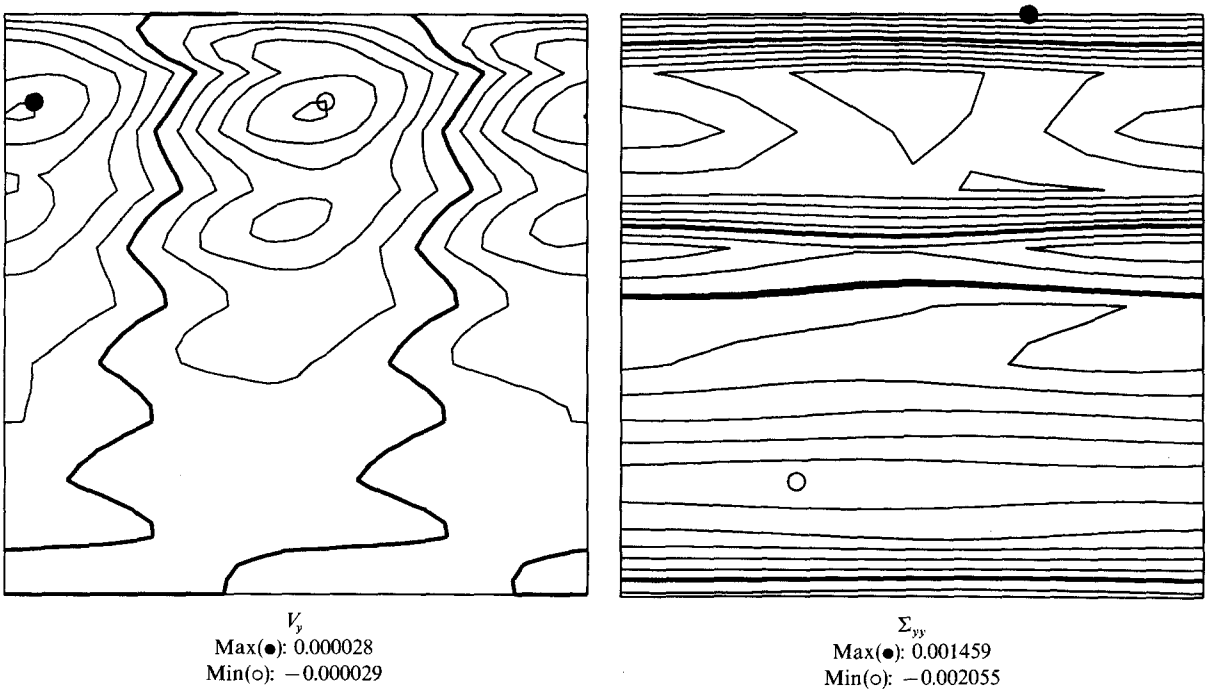

Figure 21. Components of the disturbance to the velocity (v_y) and stress (Σ_{yy}) field at $t = 25.0$ for $De = 5$ computed with the EVSS-G/SU method with $N_{el} = 10$ and $\Delta t = 0.1$. This eigenfunction is stable in time, as indicated by Figure 20. Maximum and minimum values of the functions are shown.

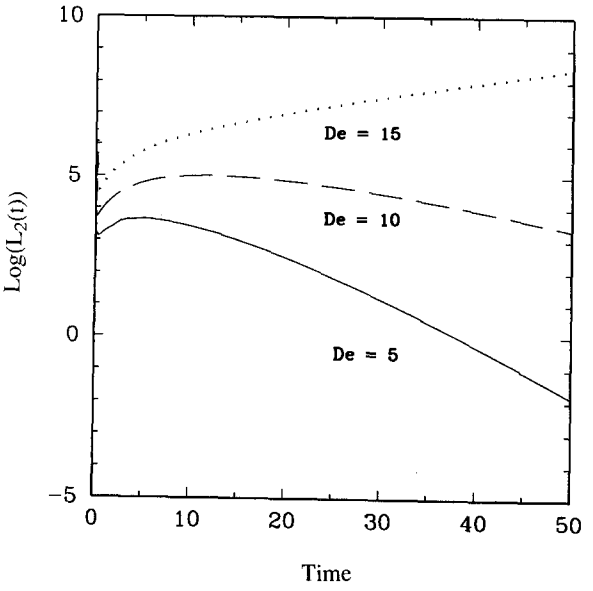

Figure 22. Transient responses, computed with the EVSS-G/GLS method, of the amplitude $L_2(t)$ defined by (28) as a function of De for the mesh $N_{el} = 10$ and $\Delta t = 0.1$.

4.6. EVSS-G/GLS Method

Stability calculations for the EVSS-G/GLS method were carried out in a manner like those described above. Interestingly, changing from SUPG to GLS methods for solution of the hyperbolic constitutive equation led to instabilities, as seen in the EEME and EVSS formulations for $De > 10$. The evolution of the disturbance, $L_2(t)$, and the form of the most dangerous eigenfunction are shown in Figures 22 and 23, respectively. The reason for the loss of stability is not understood, but must be connected to the use of the GLS method for discretization of the hyperbolic constitutive equation.

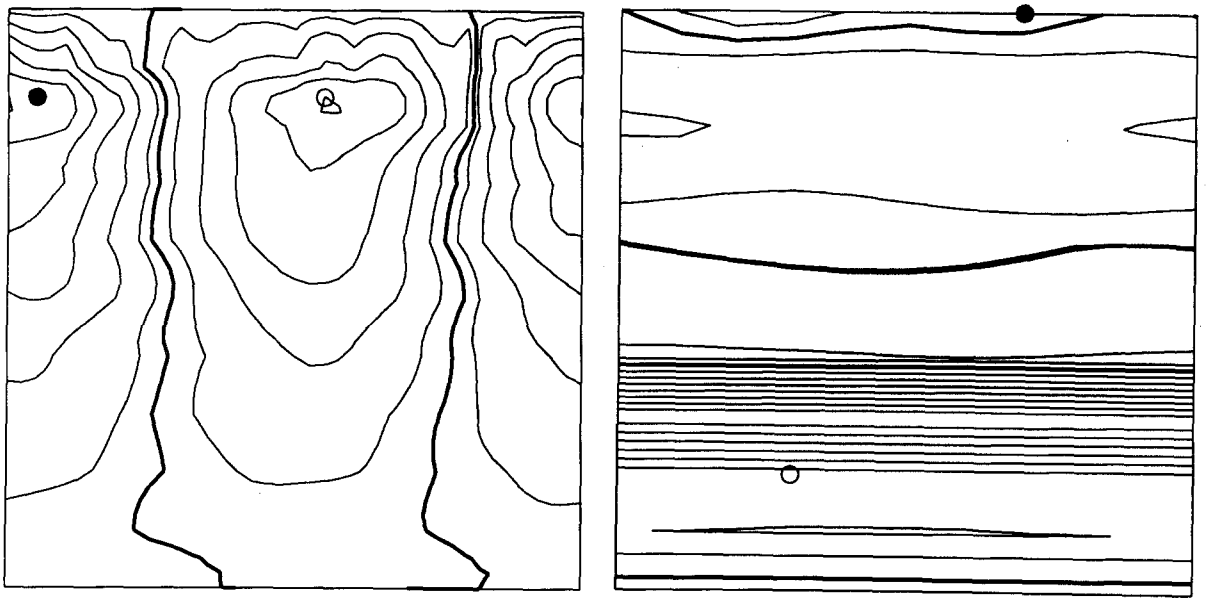

V_y
Max(●): 0.001675
Min(○): −0.001408

Σ_{yy}
Max(●): 0.178300
Min(○): −0.722300

Figure 23. Components of the disturbance to the velocity (v_y) and stress (Σ_{yy}) field at $t = 25.0$ for $De = 15$ computed with the EVSS-G/GLS method with $N_{el} = 10$ and $\Delta t = 0.1$. This eigenfunction is unstable in time, as indicated by Figure 22. Maximum and minimum values of the functions are shown.

5. Flow Around a Sphere in a Tube

The utility of the transient analysis of the linear stability of a steady-state flow is demonstrated by calculations of flow around a sphere falling in a tube, which has become an accepted test problem for the evaluation of numerical methods for viscoelastic flows (Hassager and Bisgaard, 1983; Zheng *et al.*, 1990; Lunsmann *et al.*, 1993). The difficulty of computation of steady-state flows for the UCM and OLDB models is well documented; for both models steady-state calculations seem to be only possible up to a maximum value of *De*, beyond which no solution is computed. The cause for this failure is not understood; however, calculations with viscoelastic models that predict finite growth of the elongational viscosity and shear thinning normal stresses can be continued to higher values of *De* (Chilcott and Rallison, 1988; Lunsmann *et al.*, 1993).

In the calculations presented here the EEME-P/SUPG method is used to compute the steady-state flows and transient analysis of the linear stability problem formed around these steady-states. The flow is assumed to be axisymmetric and is described in a cylindrical coordinate system centered and translating with the sphere. In this reference frame the tube wall moves past a stationary sphere with velocity $v_z = -V_s$. Dimensionless variables are defined by scaling lengths with the sphere radius R_s, velocity components with V_s, and pressure and stress components with $\eta_0 V_s/R_s$, where η_0 is the zero shear-rate viscosity of the fluid. These definitions correspond directly to the problem statement by Lunsmann *et al.* (1993); the geometry for the computational domain is shown in Figure 24. Finite-element meshes are constructed according to the procedure outlined by Lunsmann *et al.* (1993). The three meshes used here (M2, M3, M4) have approximately (2×10^4, 3.5×10^4, 5×10^4) degrees-of-freedom in each discretization.

With each mesh, calculations of steady-state flows were not possible for $De > 1.6$. The velocity components (v_r, v_z) and the shear and normal stress components (τ_{rz}, τ_{zz}) are shown in Figure 25 as a function of *De* and computed with mesh M4. The velocity field is almost unaffected by increasing *De*; however, thin boundary layers form in both components of stress adjacent to the sphere. Moreover, a wake forms in the axial normal stress τ_{zz} downstream of the sphere as *De* is increased, as a result of the strongly extensional flow created along the axis emanating from the rear stagnation point. The

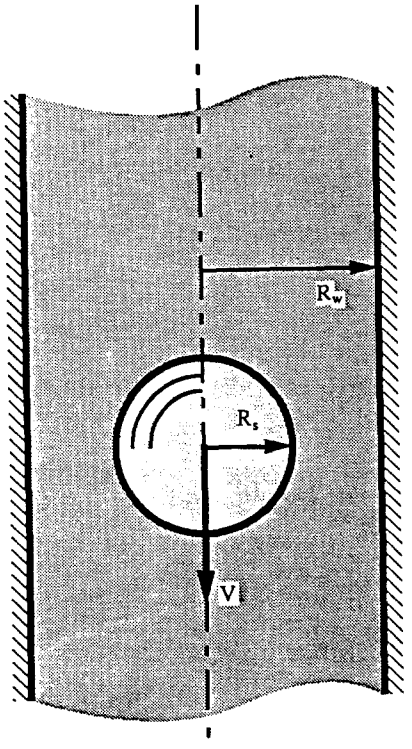

Figure 24. Geometry for a sphere falling along the axis of a vertical circular cylinder, as viewed from the reference frame of the sphere.

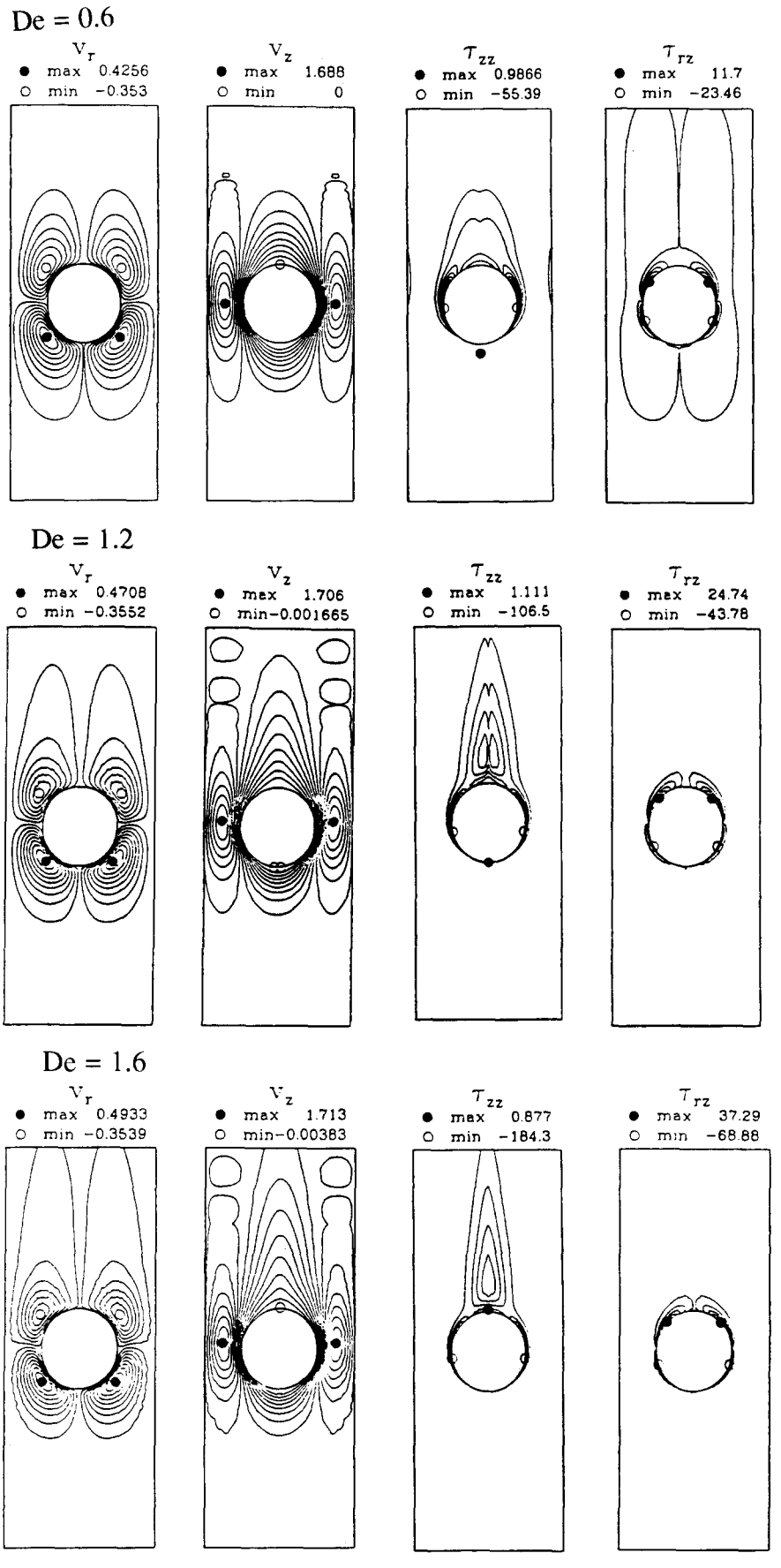

Figure 25. Sample contours of steady-state stress and velocity fields for a sphere falling along the axis of a circular tube for $R_{\text{sphere}}/R_{\text{cylinder}} = 0.5$ and $0.6 \leq De \leq 1.6$. Contours are shown for the components of the radial and axial velocity components and the shear τ_{rz} and axial normal stress τ_{zz} written in a cylindrical polar coordinate system centered along the axis of the sphere.

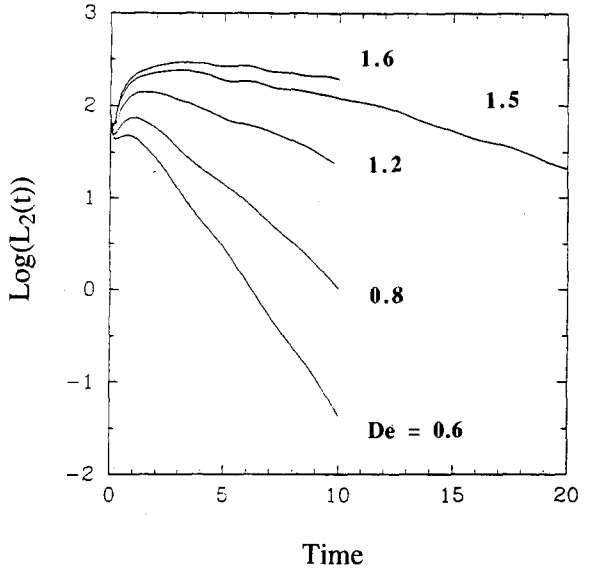

Figure 26. Transient response of the linear stability of the steady-state solutions for flow around a sphere computed with the EEME-P/SUPG method of the amplitude $L_2(t)$ defined by (28) as a function of De, $0.6 \leq De \leq 1.6$, for the mesh M2.

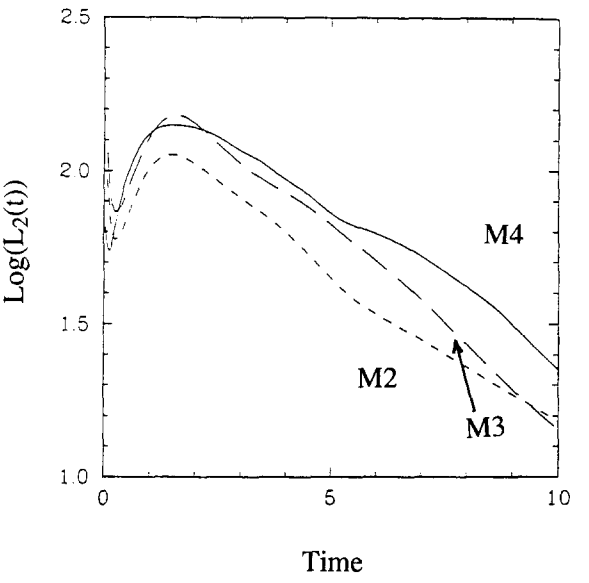

Figure 27. Transient response of the amplitude $L_2(t)$ for the linear stability of the steady-state solutions for flow around a sphere computed with the EEME-P/SUPG method as a function of the mesh for $De = 1.2$ and $\Delta t = 0.04$.

length of the stress wake increases with increasing De. There are no qualitative differences in the solution field at $De = 1.6$, where convergence of the Newton iterations is lost.

The linear stability of these steady-state solutions to random initial perturbations was tested by time integration of the linearized equations written about the steady-state solutions. The evolution of the energy in these disturbances with time is shown in Figure 26 as a function of De and computed for mesh M2 and $\Delta t = 0.04$. The flow approaches neutral stability as De is increased toward the limiting value. Similar results were produced with all three finite-element meshes. The evolution of the disturbance for $De = 1.2$ and $\Delta t = 0.04$ is shown in Figure 27 for all three meshes and differ in detail; however, some of this difference is probably attributed to the randomness of the initial condition. The decay rates at long time for the two finest meshes (M3, M4) are very similar.

The evolution of the disturbance to the stream function computed with mesh M2 is shown in Figure 28 for $De = 1.2$. The disturbance is composed of small secondary vortices that form adjacent to the sphere and move from the front to the rear. For $De \leq 1.6$, the disturbance decays in time, but approaches neutral stability as De approaches 1.6. The temporal evolution of the disturbance is shown in Figure 29 as measured by the radial velocity at the point $(r, z) = (1.2, 0)$. The most dangerous disturbance appears to remain oscillatory at $De = 1.6$, where the disturbance is just marginally stable. The failure of the steady-state calculations at $De = 1.6$ implies a limit point in the family of solutions. The linear stability calculations imply neutral stability to an oscillatory mode at this point and are not consistent with the existence of the limit point unless an oscillatory instability occurs simultaneously with the limit point, which would be a very pathological result.

The qualitative behavior of the neutral stability calculations can be compared with the laser-Doppler velocimetry (LDV) measurements of Bisgaard (1983) for the flow around a sphere falling in a tube filled with a solution of polyacrylamide and water. Bisgaard fixed the measuring volume for the LDV system and dropped the sphere, so that the velocity measurement as a function of time corresponded to the velocity at different positions in space around the sphere. Bisgaard observed that, above a critical fall velocity, the velocity field adjacent to the sphere was no longer smooth, but had undulations that corresponded to irregular variations in the velocity field that are consistent with small-scale secondary vortices adjacent to the sphere, as observed in the linear stability calculations described above. Because of the experimental method, it is not possible to decide whether the

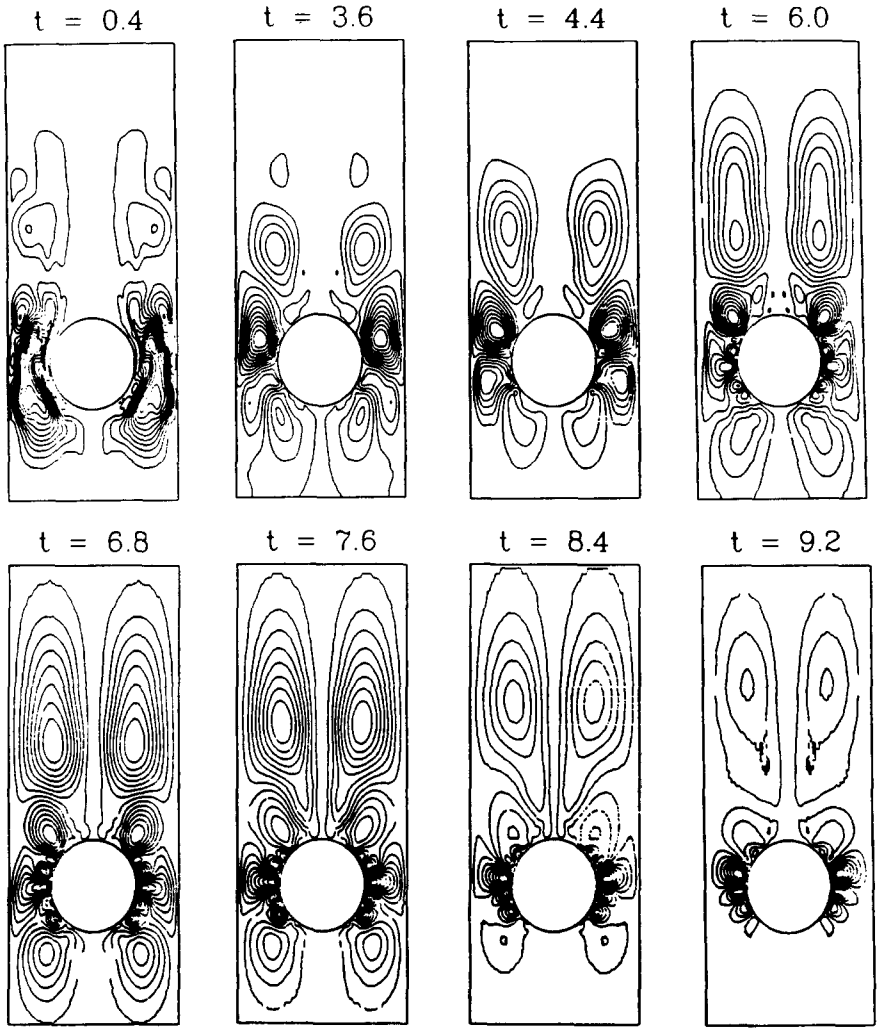

Figure 28. Temporal response of the stream function for $De = 1.2$ and $\Delta t = 0.04$ as a function of time, as computed for the linear stability of the flow around a sphere with mesh M4 and the EEME-P/SUPG method.

perturbations observed by Bisgaard are stationary around the sphere or translate, as observed in the linear-stability calculations.

6. Discussion

Above all, the calculations described here establish the difficulty with the temporal stability of finite-element methods for the solution of viscoelastic flows. Numerical calculation of the linear stability of the planar Couette flow is an excellent problem for establishing temporal stability because the behavior of the most dangerous eigenvalue and the structure of the eigenfunction are known analytically from Gorodstov and Leonov (1967). The results demonstrated here show that algorithms like the EEME/SUPG and EVSS/SUPG, which give accurate and numerically stable results for smooth steady-state flows, are limited by numerical instabilities for time-dependent calculations. The instabilities are linked to the very difficult problem associated with accurate calculation of the eigenvalue spectrum for simple shear flow. The most dangerous eigenvalue has a real part that approaches $-1/2De$ and an imaginary part that scales as k, where k is the streamwise wave number, for $De \gg 1$; moreover, the eigenfunction develops boundary layer structure in the cross-stream direction. It is hard to imagine a more difficult problem to resolve.

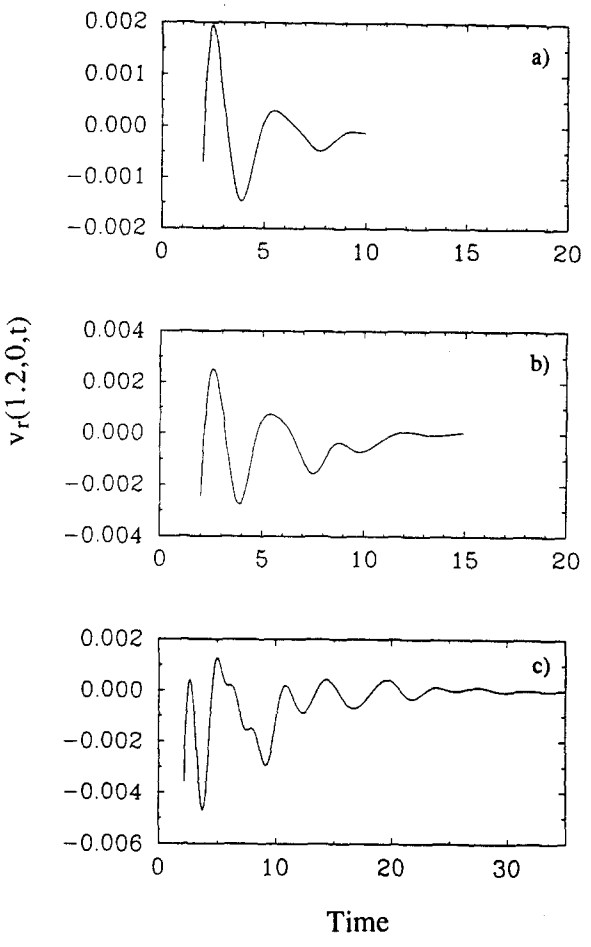

Figure 29. Transient response of the radial velocity at a position next to the equator of the sphere $(r, z) = (1.2, 0)$ for mesh M2 and $\Delta t = 0.04$. Results are shown for *De* of (a) 0.6, (b) 1.2, and (c) 1.6. The approach to neutral stability is apparent.

Because fully implicit integration methods are used for solving the constant coefficient linear equation sets that result for the linear-stability formulation, the issue of numerical stability of the time integration is directly related to the spatial discretization. The instability seen in the EEME/SUPG and EVSS/SUPG methods is related to numerical instabilities that are inherent to these formulations. The calculations reported in Section 4.1 show that the energy in the most dangerous disturbance is concentrated near a stationary streamline. This fact led us to conclude that the numerical instability was related to the compatibility of the finite-element spaces for velocity gradient and stress in the limit where the constitutive equation reduces to an algebraic equation between these variables.

The EVSS-G formulation uses an independent interpolation of the components of the velocity gradient tensor constructed so as to give compatible approximations for the velocity gradient and deviatoric stress. The three numerical methods constructed with the EVSS-G mixed method, EVSS-G/SUPG, EVSS-G/SU, and EVSS-G/GLS, all appear to have much greater numerical stability than the orginal mixed finite-element methods. In two cases, EVSS-G/SUPG and EVSS-G/SU, no upper bound was found for the loss of stability in the plane Couette flow analysis up to $De = 50$. Because no numerical stability limit was identified with these methods, Keiller's idea (1992) that the onset of numerical instability, as seen in his finite-difference discretizations, was connected with poor cross-stream resolution relative to the streamwise direction could not be tested in the context of our calculations with the EVSS-G methods, because no instability could be found. Possibly, the instability exists at higher values of *De*. Alternatively, Keiller's results may also be caused by the application of incompatibile finite difference approximations for velocity gradients and stresses and would disappear with proper discretization.

Much is left to be done in order to develop the EVSS-G mixed finite-element methods into a robust family of techniques. The computations described here do not address important questions

about the applicability of these numerical methods to the solution of flows with singularities, such as sharp corners in solid surfaces or static or moving contact lines at the junctions of solid surfaces with free surfaces. We believe that these problems require attention to the well-posedness of the boundary-value problem formed by the particular constitutive equation, as well as careful design of the numerical method. The calculations of Coates *et al.* (1992) for constitutive models with Newtonian-like behavior near a sharp corner in a solid wall demonstrate this coupling.

The efficiency of time-dependent computations would be greatly enhanced by replacing the fully implicit time-integration methods applied by Northey *et al.* (1990) and used here by time-splitting methods that solve the discrete form of the constitutive equation and the momentum/continuity pair separately, especially if the constitutive equation can be solved by explicit methods. New attempts at developing such methods are underway.

Calculations for the linear stability of the flow around a sphere falling in a tube using the EEME-P/SUPG method give the first indication of the presence of complex dynamics that may evolve from complex steady-state flows computed with simple differential constitutive models. These calculations show that the most dangerous eigenfunction for the UCM model corresponds to a layer of axisymmetric vortices that lay in the stress layer adjacent to the sphere and which move from the fore to the aft of the sphere with time. Although this result is qualitatively similar to the experimental observations of Bisgaard (1983) for instability around a sphere, more experimental and computational work needs to be done before a definite connection can be made.

References

Apelian, M.R., Armstrong, R.C., and Brown, R.A. (1988) Impact of constitutive equation and singularity on the calculation of stick-slip flow: the modified upper-convected Maxwell fluid. *J. Non-Newtonian Fluid Mech.*, **27**, 299–321.

Baijens, F.T.P. (1992) Application of Galerkin-least-squares related methods to the mixed formulations of steady viscoelastic flow. *J. Non-Newtonian Fluid Mech.*, submitted.

Baranger, J., and Sandri, D. (1991a) Approximation par finis d'ecoulements de fluides viscoelastiques: Existence de solutions approchees er majoration d'erreur. I. Constraintes discontinues, *C. R. Acad. Sci. Paris Sér. I*, **312**, 541–544.

Baranger, J., and Sandri, D. (1991b) Approximation par finis d'ecoulements de fluides viscoelastiques: Existence de solutions approchees er majoration d'erreur. II. Constraintes continues. *C.R. Acad. Sci. Paris Sér. I*, **313**, 111–114.

Beris, A.N., Armstrong, R.C., and Brown, R.A. (1987) Finite-element/spectral calculations of the flow of a Maxwell fluid between eccentric rotating cylinders. *J. Non-Newtonian Fluid Mech.*, **22**, 129–167.

Bisgaard, C. (1983) Velocity fields around spheres and bubbles investigated by laser-Doppler anemometry, *J Non-Newtonian Fluid Mech.*, **12**, 282–302.

Brezzi, F., and Fortin, M. (1991) *Mixed and Hybrid Finite Element Methods.* Series in Computational Mechanics, Springer-Verlag, New York.

Brooks, A.N., and Hughes, T.J.R. (1982) Streamline upwind/Petrov Galerkin formulations for convection dominated flows with particular emphasis on the incompressible Navier–Stokes equations. *Comput. Methods Appl. Mech. Engrg.*, **32**, 199–259.

Brown, R.A., Armstrong, R.C. Beris, A.N., and Yeh, P.-W. (1986) Finite element analysis of complex viscoelastic flows. *Comput. Methods Appl. Mech. Engrg.*, **58**, 201–226.

Burdette, S., Coates, P.J., Armstrong, R.C., and Brown, R.A. (1989) Finite element calculation of viscoelastic flow through an axisymmetric corrugated tube using the explicitly elliptic momentum equation formulation (EEME). *J. Non-Newtonian Fluid Mech.*, **33**, 1–23.

Carey, G.F., and Oden, J.T. (1986) *Finite Elements*, Vols. 4 and 6. Prentice-Hall, Englewood-Cliffs, NJ.

Chilcott, M.D., and Rallison, J.M. (1988) Creeping flow of dilute polymer solutions past cylinders and spheres. *J. Non-Newtonian Fluid Mech.*, **29**, 381–432.

Coates, P.J., Armstrong, R.C., and Brown, R.A. (1992) Calculation of steady-state viscoleastic flow through axisymmetric contractions using the EEME formulation. *J. Non-Newtonian Fluid Mech.*, **42**, 141–188.

Crochet, M.J., Davies, A.R., and Walters, K. (1984) *Numerical Simulation of Non-Newtonian Flow.* Elsevier, Amsterdam.

Dupret, F., Marchal, J.M., and Crochet, M.J. (1985) On the consequence of discretization errors in the numerical calculation of viscoelastic flow. *J. Non-Newtonian Fluid Mech.*, **18**, 173–186.

Franca, L.P., Frey, S.L., and Hughes, T.J.R. (1992) Stabilized finite element methods: I. Application to the advective–diffusive model. *Comput. Methods Appl. Mech. Engrg.*, **95**, 253–276.

Gorodstov, V.A., and Leonov, A.I. (1967) On a linear instability of plane parallel Couette flow of viscoelastic fluid. *J. Appl. Math. Mech.*, **31**, 289–299.

Hassager, O., and Bisgaard, C. (1983) A Lagrangian finite element method for the simulation of flow of non-Newtonian liquids. *J. Non-Newtonian Fluid Mech.*, **12**, 153–164.

Hughes, T.J.R., Franca, L.P., and Hulbert, G.M. (1989) A new finite element formulation for computational fluid dynamics. VIII. The Galerkin least-squares method for advective–diffusive equations. *Comput. Methods Appl. Mech. Engrg.*, **73**, 173–189.

Johnson, C., Nävert, U., and Pitkaranta, J. (1984) Finite element methods for linear hyperbolic problems. *Comput. Methods Appl. Mech. Engrg.*, **45**, 285–312.

Joseph, D.D., Renardy, M., and Saut, J.C. (1985) Hyperbolicity and change of type in the flow of viscoelastic fluids. *Arch. Rational Mech. Anal.*, **87**, 213–251.

Keiller, R.A. (1992) Numerical instability of time dependent flows. *J. Non-Newtonian Fluid Mech.*, **43**, 229–246.

King, R.K., Apelian, M.R., Armstrong, R.C., and Brown, R.A. (1988) Numerically stable finite-element methods for solution of steady viscoelastic flows. *J. Non-Newtonian Fluid Mech.*, **29**, 147–216

Leborgne, G. (1992) Simulation numerique d'ecoulements de fluides viscoelasticques de type Oldroyd: utilisation d'element finis de degre 1. Doctoral thesis, l'Ecole Poltechnique, Paris.

Lee, K., and Finlayson, B.A. (1986) Stability of plane Poiseuille flow and Couette flow of a Maxwell fluid. *J. Non-Newtonian Fluid Mech.*, **21**, 65–78.

Lunsmann, W.J., Genieser, L., Armstrong, R.C., **and** Brown, R.A. (1993) Finite element analysis of steady viscoelastic flow around a sphere in a tube: calculations with constant viscosity models. *J. Non-Newtonian Fluid Mech.*, in press.

Marchal, J.M., and Crochet, M.J. (1987) A new mixed finite element method for calculating viscoelastic flow. *J. Non-Newtonian Fluid Mech.*, **26**, 77–114.

Mendelson, M.A., Yeh, P.-W., Brown, R.A., and Armstrong, R.C. (1982) Approximation error in finite element calculation of viscoelastic fluid flows. *J. Non-Newtonian Fluid Mech.*, **10**, 31–54.

Northey, P., Armstrong, R.C., and Brown, R.A. (1990) Finite element calculations of time-dependent two-dimensional flows of an upper-convected Maxwell fluid using the EEME formulation. *J. Non-Newtonian Fluid Mech.*, **36**, 109–134.

Northey, P., Armstrong, R.C., and Brown R.A. (1992) Finite amplitude time-periodic states in viscoelastic Taylor–Couette flow of a UCM fluid. *J. Non-Newtonian Fluid Mech.*, **42**, 117–140.

Pilitsis, S., and Beris, A.N. (1989) Calculations of steady-state viscoelastic flow in an undulating tube. *J. Non-Newtonian Fluid Mech.*, **31**, 231–287.

Rajagopalan, D., Armstrong, R.C., and Brown, R.A. (1990a) Finite element analysis of viscoelastic flow of a multi-mode Maxwell fluid: application of EEME formulation. *J. Non-Newtonian Fluid Mech.*, **36**, 135–158.

Rajagopalan, D., Armstrong, R.C., and Brown, R.A. (1990b) Finite element methods for calculation of viscoelastic flow for constitutive equations with a Newtonian viscosity. *J. Non-Newtonian Fluid Mech.*, **36**, 159–192.

Renardy, M. (1985) Existence of slow steady flows of viscoelastic fluids with differential constitutive equations. *Z. Angew. Math. Mech.*, **65**, 449–451.

Renardy, M., and Renardy, Y. (1986) Linear stability of plane Couette flow of an upper convected Maxwell fluid. *J. Non-Newtonian Fluid Mech.*, **22**, 23–33.

Renardy, M., Hrusa, W.J., and Nohel, J.A. (1987) *Mathematical Problems in Viscoelasticity*. Longmans, New York.

Rutkevich, I.M. (1970) The propogation of small perturbations in a viscoelastic fluid. *J. Appl. Math. Mech.*, **34**, 35–50.

Rutkevich, I.M. (1972) On the thermodynamic interpretation of the evolutionary conditions of the equations of the mechanics of finitely deformable viscoelastic media of Maxwell type. *J. Appl. Math. Mech.*, **36**, 283–295.

Zheng, R., Phan-Thien, N., and Tanner, R.I. (1990) On the flow past a sphere in a cylinderical tube: limiting Weissenberg number. *J. Non-Newtonian Fluid Mech.*, **36**, 27–49.